machines

MDPI

Article

Development of a Restraint System for Rear-Facing Car Seats

Samet Yavuz [1] and Selcuk Himmetoglu [2,*]

[1] Institute of Science, Hacettepe University, Beytepe, Ankara 06800, Türkiye; syavuz@thk.edu.tr
[2] Mechanical Engineering Department, Hacettepe University, Beytepe, Ankara 06800, Türkiye
* Correspondence: s.himmetoglu@hacettepe.edu.tr

Abstract: In self-driving vehicles, passengers can set their seats in an unconventional seating position, such as rear-facing. Sitting in such an orientation can increase the risk of whiplash in the head-and-neck system in a frontal impact, as frontal crashes usually have higher severities compared with rear-end crashes. This paper shows that a forward-facing front seat optimised for rear-impact protection needs to be redesigned to be used as a rear-facing seat. In the second and main part of this paper, a restraint system for rear-facing car seats is developed, and frontal impact simulations with 64 km/h of delta-V are used to evaluate its performance. The designed seating system comprises two rigid torso plates, a fixed recliner and an energy absorber under the seat pan. Without using the developed restraint system, the 50th percentile male human model is exposed to neck shear forces exceeding 600 N. With the developed restraint system, neck shear forces are less than 350 N in frontal impacts with 64 km/h of delta-V. Apart from whiplash, the risk of head, chest, lower extremity and lower back injuries are also evaluated. The results confirm that the developed restraint system successfully protects the occupant since all assessment criteria values are lower than the injury assessment reference values.

Keywords: autonomous vehicle crashes; rear-facing seat; whiplash

Citation: Yavuz, S.; Himmetoglu, S. Development of a Restraint System for Rear-Facing Car Seats. *Machines* **2023**, *11*, 1076. https://doi.org/10.3390/machines11121076

Academic Editors: Walter D'Ambrogio and Konrad Jan Waluś

Received: 15 October 2023
Revised: 30 November 2023
Accepted: 6 December 2023
Published: 8 December 2023

1. Introduction

In self-driving cars (autonomous cars), occupants will opt for various seating positions, with seats oriented in different directions within the car. However, the current restraint systems (seatbelt, airbag, seat, head restraint) have been developed and optimised for the conventional seating plan involving only forward-facing seats. Therefore, any change in the seating plan requires a redesign of the traditional restraint systems (protection systems). In road traffic accidents, whiplash causes discomfort and pain in the head and neck, which occur typically in rear-end collisions, and whiplash-associated disorders are the consequences of whiplash. Occupants sitting in forward-facing seats have the highest risk of whiplash-associated disorders in rear-end crashes [1–3]. The majority of rear-end crashes happen with delta-V lower than 25 km/h [1–3]. According to the National Automotive Sampling System-Crashworthiness Data System (NASS-CDS), between the years 1994–2015, 98% of rear-end crashes in the United States occurred with delta-V lower than 35 km/h [4]. Delta-V is the change in the velocity of the struck vehicle due to impact, and crash pulse refers to the acceleration versus time history of the vehicle being struck. The European New Car Assessment Programme (EuroNCAP) employs dynamic and static assessment of forward-facing front seats corresponding to the conventional seating plan to evaluate the rear impact performance of seats [5]. EuroNCAP applies medium and high-severity rear-impact crash pulses with delta-Vs of 16 km/h and 24 km/h, respectively, in the dynamic whiplash test [5].

Occupants in autonomous vehicles are expected to have the option of sitting in rear-facing seats; however, these occupants will be at a higher risk of whiplash in frontal impacts, which statistically occur with much higher severities in comparison to rear-end collisions. As an example, in the United States New Car Assessment Programme (US

NCAP), cars impact a fixed rigid wall with 100% overlap at an impact speed of 56 km/h, which corresponds to a frontal impact with a delta-V of around 64 km/h [6]. Hence, a rear-facing seat has to cope with higher crash energies in frontal impacts and this can lead to other problems (head and torso injuries) together with whiplash-associated disorders.

Whiplash-mitigating forward-facing front seats were first introduced into the market in the late 1990s. The Whiplash Protection System (WHIPS) of the Volvo and the Self-Aligning Head Restraint (SAHR) of the Saab are the leading anti-whiplash seats developed during that time [7,8]. Since then, all anti-whiplash seats (forward-facing front seats) in the market have benefited from the design principles applied in WHIPS and SAHR. During a rear-end collision, WHIPS absorbs the energy of the occupant as the seatback first translates and then rotates backward with the aid of a recliner mechanism. The plastic deformation in the recliner makes the seatback compliant and this lowers the load on the torso, hence reducing the motion of the head relative to the upper torso. SAHR employs a stiff seatback frame together with a reactive head restraint that is moved upward and forward to provide early head support. This limits head motion relative to the upper torso. In the last 10 years, crash-adaptive anti-whiplash seats have been introduced that provide balanced protection across a wide range of crash severities [1,9] by using energy absorbers with varying breakaway forces/torques and damping coefficients in the recliner and under the seat pan.

Development of new restraint systems for autonomous vehicles has started in the last four years; however, a review of the literature reveals very few studies on rear-facing occupants subjected to frontal impacts. In a preliminary study [10], the German In-Depth Accident Study (GIDAS) database was searched for frontal collisions that involved adult passengers in rearward-facing seats. Five cases with a delta-V of 25 km/h or lower were found, in which the passengers did not sustain any whiplash-associated disorders. In two cases, the passengers sat on special rear-facing seats in ambulances; these seats had almost upright seatbacks to protect the patient. It has been shown [1] that seats providing close support to the upper torso (by the seatback) and the head (by the head restraint) can reduce whiplash risk significantly.

Zellmer and Manneck [11] carried out frontal impact sled tests by applying crash pulses with delta-V of up to 60 km/h by employing Hybrid III dummies placed on a rear-facing seat. In their first test, they used a production seat that was subjected to a crash pulse representing a frontal collision at an impact speed of 40 km/h; this seat showed excessive deformation. Subsequently, they constructed an experimental generic seat with two seatbelts secured to a frame mounted on a sled to restrict the rearward rotation of the seatback and adjust energy dissipation by the seat. In this generic seat, they also fixed the head of the dummy to the head restraint to remove the gap between the head and the head restraint. In these tests, various injury measures corresponding to chest, neck, head, legs and lumbar spine were evaluated and it was observed that the head and chest acceleration and the compression forces on the lumbar spine were close to the injury threshold values. In the sled tests, a Hybrid III dummy, which was designed for use in frontal impact tests of forward-facing seats, was employed; moreover, the generic seat did not represent a typical production seat. In a subsequent study [12], this experimental generic seat was modelled to include a fixed recliner and then crash simulations were performed using SAFER-HBM human-body model, THOR and Hybrid III dummy models to evaluate the differences in the responses of these human body models.

In another study [13], rotatable seats designed for autonomous vehicles were studied where the seats were rotated quickly to a favourable position in the pre-crash phase to minimise injuries. A rigid-seat model where the surfaces are covered with foam, was used. A human model created using the finite element (FE) method was used together with this rigid seat. At different seating orientations, the seat-occupant model was subjected to frontal impacts with a delta-V of 56 km/h. The results indicated that the passenger in the rear-facing seat was safer in comparison to those in other seating orientations. However, this study did not involve an evaluation of whiplash risk.

Total Human Model for Safety (THUMS) FE human-body model and FE models of two production seats were utilised in another study [14] to study seat-occupant behaviour in rear-end crashes with delta-Vs of 24 km/h and 56 km/h. Only head and chest injury risks were evaluated. In this study, seats with compliant and fixed recliners were compared using simulations in which the torso of the occupant loaded the seatback. The results showed that chest and head injury metric values were reduced when a fixed recliner was used. Head injury metric values and chest deflection increased when the initial seatback recline angle was increased. The authors concluded that injury risks were mitigated by the use of an active head restraint, an integrated seatbelt and a fixed recliner.

In the first part of this paper, an advanced forward-facing front seat for whiplash mitigation is presented. Its performance is optimised for crash pulses with delta-Vs ranging from 9.4 km/h to 24 km/h by using a biofidelic 50th percentile male human model [15,16]. This forward-facing front seat can earn maximum points from all 10 whiplash assessment criteria in the EuroNCAP whiplash protocol [5] hence it mitigates whiplash significantly considering that the majority of rear impacts occur with delta-Vs lower than 25 km/h [4]. When this forward-facing seat is reversed for use as a rear-facing seat and frontal impact conditions are applied with crash severities higher than that of EuroNCAP's high severity rear-impact crash pulse, the seat performs poorly, leading to high whiplash risk. Therefore, in the second part of the paper, an improved design for rear-facing seats, which comprises two rigid torso plates that extend from the seatback to the thorax and lumbar sections of the human torso, is presented. This improved design also includes an energy absorber under the seat pan, a head restraint and a fixed recliner to prevent excessive rotation of the seatback at higher crash severities. This improved design protects the head, neck and torso of the occupant successfully in frontal impacts with delta-Vs as high as 64 km/h. The torso plates and the head restraint help to restrict the motion of the head, neck and torso relative to the seatback. This paper is one of the outputs from the PhD thesis study of the first author.

The concept of using torso plates was first suggested in a preliminary study by Himmetoglu [1], where the rear-facing seat included energy absorbers in the recliner and underneath the seat pan and two torso plates extended from the seatback. The amount of damping and the breakaway forces/torques in the energy absorbers were varied to adapt the seat to frontal impacts with diverse severities. Although the loads on the occupant from this seat were low in comparison to the injury assessment reference values, it had a complex design since it required the estimation of crash severity just before the collision. Moreover, the vertical and pitch motion of the car were not taken into account in frontal crashes with delta-Vs higher than 40 km/h. Detailed evaluation of injury risks, assessment of chest deflection, lower extremity and pelvis injuries and out-of-position (occupant leaning forward) cases were also not included in that previous study [1].

In designing the seats in this study, heuristic optimisation based on trial-and-error and engineering judgement is used. This helps to master, understand and interpret the dynamics of the system. This method of optimisation is a very educative tool. The seat model used in this study has the geometry of a typical seat to accommodate the occupant. Optimisation is applied to derive the required mechanical properties of the recliner mechanism, energy absorbers underneath the seat pan and the foams used in the seatback, seat pan and head restraint.

2. Forward-Facing Front Seat for Whiplash Mitigation

This section describes previously unpublished technical and modelling details of an advanced forward-facing anti-whiplash front seat and its dynamic assessment using the EuroNCAP criteria.

2.1. Design Principles and Modelling Details of the Seat

The advanced forward-facing anti-whiplash front seat, designed to be used in the conventional seating plan, is shown in Figure 1. The seat comprises a typical head restraint

(HR), seat pan (SP), seatback (SB), recliner mechanism (R), 3-point seatbelt and an energy absorber (D) beneath the seat pan. This seat is designed by employing a biofidelic 50th percentile male human-body model [15,16], as shown in Figure 1. The human-body model represents an initially relaxed occupant who is unaware of the incoming rear impact. The MSC Visual Nastran software was used to build the multi-body seat-occupant model. The human-body model is not distributed with MSC Visual Nastran; it is specifically built to design seats that can reduce whiplash risk and is calibrated using volunteer data from JARI (Japanese Automobile Research Institute) rear impact sled tests [17]. Figure 1 shows the typical driving posture (normal sitting posture) of the occupant (human-body model) prior to rear impact. The backset (the horizontal distance between the head restraint and the head) in this initial posture is 5.8 cm and the head restraint is high enough to cover the head completely. The initial posture of the human-body model represents the normal sitting posture in the front seat, with the back pressed against the seatback and the head looking forward. This initial posture of the human-body model is comparable to that of the BioRID dummy used in the EuroNCAP dynamic whiplash tests and the design torso angle of the seat is 20 deg from the vertical [5]. The initial posture of the human-body model is derived from 50th percentile male volunteers in JARI (Japanese Automobile Research Institute) rear impact sled tests. These JARI volunteer tests were used in the past to validate the BioRID dummy [17]. In the initial positioning of the human-body model, the head restraint is positioned to have good geometry, as specified in the IIHS (Insurance Institute for Highway Safety) Vehicle Seat/Head Restraint Evaluation Protocol [18]. The initial angle of the seatback is approximately equal to the torso angle (20 deg from vertical), which is close to the seatback angle most preferred (between 21 and 22 deg) by front seat occupants [19,20].

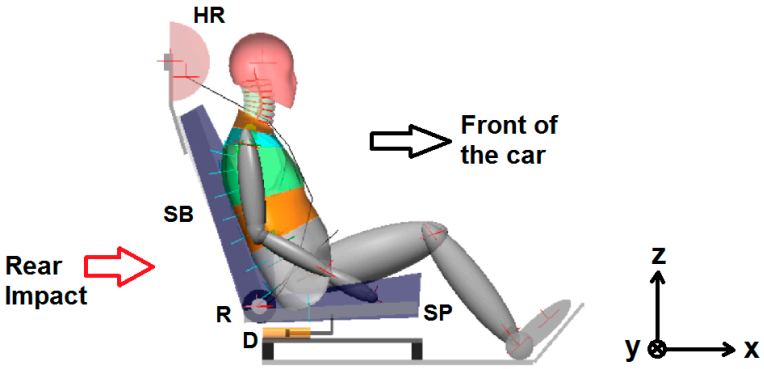

Figure 1. Forward-facing anti-whiplash front seat. The inertial frame is shown on the right.

This forward-facing anti-whiplash front seat utilises state-of-the-art occupant protection technology. In case of a rear impact, the recliner mechanism (R) undergoes plastic deformation that makes the seatback (SB) rotate and absorb crash energy. The recliner mechanism, which behaves like the load limiters in seatbelt retractors, also incorporates a breakaway element. At the start of the collision, this breakaway element generates high resistance to seatback rotation in order to couple the torso to the seatback quickly and to prevent excessive rotation of the seatback. Hence, the breakaway element functions like the pretensioners used in seatbelt systems. Figure 2 shows the variation in the dynamic torque generated by the recliner mechanism versus the seatback angle (rotation) for rear impacts with delta-Vs ranging from 13 km/h to 24 km/h. When the seatback angle reaches 21 deg, the stiffness of the recliner mechanism increases as it bottoms out, as seen in Figure 2. The variation in dynamic torque at the recliner mechanism, shown in Figure 2, is similar to those of some production seats reported in [21].

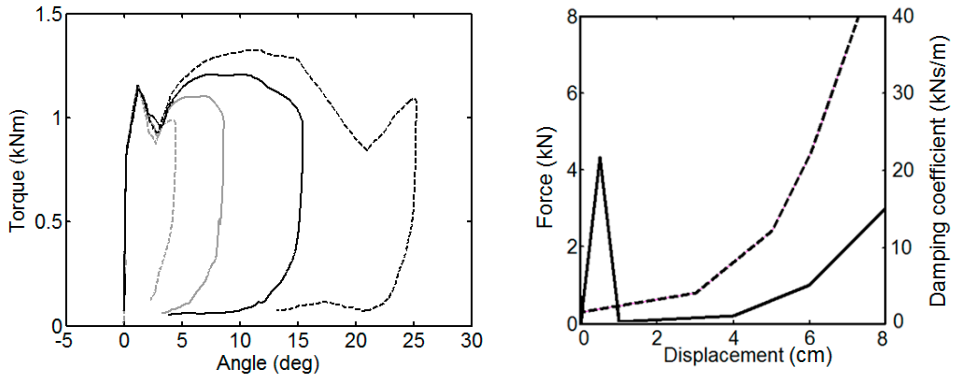

Figure 2. (**a**) Dynamic torque generated by the recliner mechanism; (**b**) Mechanical characteristics of the energy absorber (D). The solid curve shows stiffness and the dashed curve shows damping [9].

The energy absorber (D), which was designed in a previous study [9], consists of a nonlinear spring installed in parallel with a viscous damper; their characteristics are given in Figure 2. The energy absorber also possesses a breakaway element to prevent its activation in normal driving and for rear impacts with delta-V's lower than 10 km/h. In the rebound phase of seat-occupant motion, the forward rebound of the seat pan (SP) is limited as the energy absorber employs high damping (30 kNs/m) during forward movement (towards the front of the car) of the seat pan.

When the severity of the rear-end collision is low (around 10 km/h of delta-V), only the breakaway element of the recliner mechanism is broken and as a result, only the seatback rotates to cushion the load on the torso. For delta-Vs higher than >10 km/h, the breakaway elements in the recliner mechanism and the energy absorber (D) are both broken. When the breakaway element in the energy absorber is also broken, the energy absorber immediately starts to absorb energy and prevents the seatback from rotating away from the upper torso. Therefore, in the early stages of impact, the seat pan quickly moves rearward to help the torso lean on the seatback. In rear-end collisions with delta-Vs higher than 10 km/h, the prompt activation of the seat pan and the presence of the recliner breakaway element initiate the leaning of the torso and the head on the seatback and head restraint, respectively, thus the rearward movement of the seat pan and the breakaway torque in the recliner mechanism operate like the double pretensioners used in seatbelt systems. As a result, the torso and the head are coupled to the seatback and the head restraint, respectively. The seatback foam is designed to be compliant, such that the head of the occupant makes early contact with the head restraint as the torso displaces into the seatback structure in the first 50 ms of collision. The initial backset (5.8 cm) before the impact provides the head with comfort; this backset value is in accordance with the amount of seatback foam compliance to provide early head contact times between 47 ms and 62 ms.

In the ensuing stages of the collision, the energy absorber (D) and the recliner mechanism collaborate to share the crash energy to optimally limit the loading on the torso, including high-severity rear impacts. The compliances and thicknesses of head restraint foam and seatback foam and suspension are tailored using rear impact simulations to limit the relative motion between the head and upper torso, while the head and torso displace into the head restraint and seatback, respectively. For instance, if the seatback foam bottomed out quickly due to a small thickness while at the same time the head restraint foam was both thick and very soft, the head would retract and extend with respect to the upper torso, causing neck injuries. The amount of energy absorbed by the head restraint is also associated with its thickness. During rear impact, the foam and suspension of the seatback allow the torso to displace into the seatback structure by a maximum of 5 cm. The foam of the head restraint is 8 cm in thickness. Seat pan foam deformation is at most 4 cm before

it bottoms out. The key elements of the forward-facing seat design are the breakaway elements that provide efficient crash-energy absorption.

The retractor of the seatbelt system contains a vehicle sensor mechanism that locks the seatbelt webbing during sudden acceleration or deceleration of the vehicle; hence, this locking mechanism is sensitive to the acceleration and deceleration of the vehicle. This mechanism works separately from the webbing sensor mechanism that locks the seatbelt when the webbing is pulled quickly. Together with the webbing sensor mechanism, this vehicle sensor mechanism suppresses seatbelt extension, limits the ramping of the occupant along the seatback, reduces the rebound displacement of the torso and limits the forward motion of the pelvis in the rebound phase.

Figure 3 shows the total dynamic force on the seatback versus the total deformation of seatback foam and suspension at the high-severity rear-impact crash pulse TR(24) where the total dynamic force on the seatback is measured by pressure sensors in the model and the total deformation of seatback foam and suspension is measured around the spinous process of the 8th thoracic vertebra of the human model. The compliance of the seatback foam and suspension is uniform throughout the seatback. The total dynamic force on the seat pan versus the deformation of the seat pan foam at pulse TR(24) where the total dynamic force is measured by pressure sensors and the deformation of seat pan foam is measured around the inferior end of the ischium of the pelvis is shown in Figure 3. The compliance of seat pan foam is uniform throughout the seat pan. The deformations shown in Figure 3 are dynamic, hence they are measured from static equilibrium. The dynamic force versus dynamic deformation characteristics, shown in Figure 3, are representative of typical foams used in automotive seatings [22]. Figure 4 shows the total dynamic force (normal to the head restraint) versus the deformation behaviour of the head restraint foam in the model derived from the dummy head form impactor tests [23,24]. The dashed lines in Figure 4 correspond to the hysteresis slope used in the modelling of hysteresis behaviour in foams [25].

Design optimisation of the seat is achieved by applying the five crash pulses specified in Table 1 where the corresponding peak acceleration (a_{peak}), delta-V and peak moving average acceleration (a_{m50}) (time window 50 ms) [26] are presented. It has been shown [27–29] that other than delta-V, the peak moving average acceleration of the occupant compartment and especially the shape of the crash pulse are highly influential in injury risk. The crash pulses SN(16) and TR(24) are the only pulses employed in the EuroNCAP whiplash protocol [5] and are medium and high-severity rear-impact crash pulses, respectively. The crash pulses SN(9.4), SN(13) and SN(20) are taken from reference [9]. The crash pulses denoted by SN and TR are sinusoidal and trapezoidal in shape. The crash pulses are applied along the x-axis (i.e., horizontally) of the inertial frame shown in Figure 1.

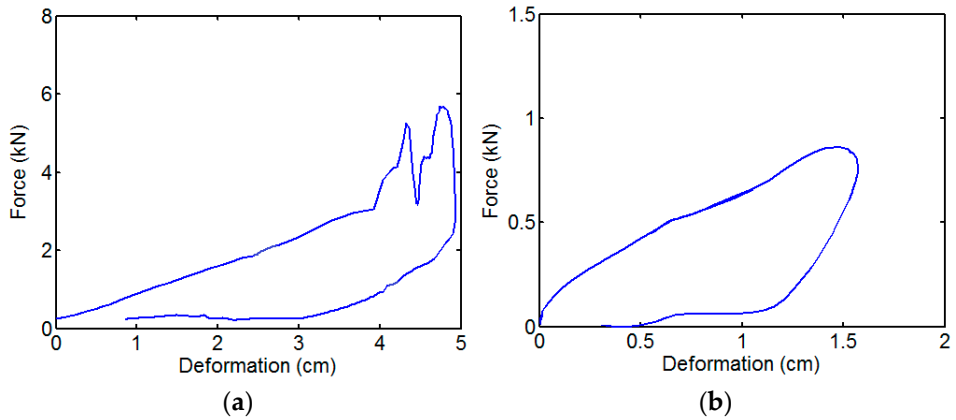

Figure 3. Dynamic force versus dynamic deformation characteristics at the high-severity rear-impact crash pulse TR(24): (**a**) Seatback foam and suspension; (**b**) Seat pan foam.

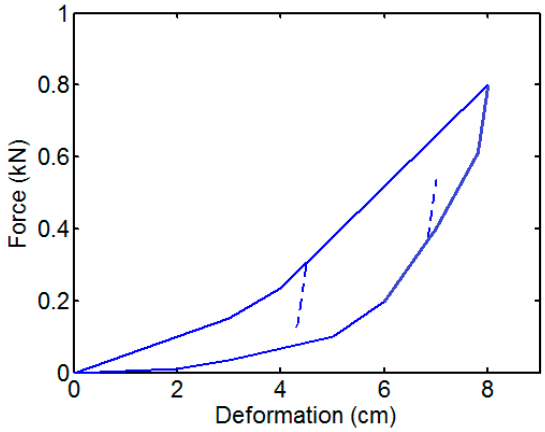

Figure 4. Dynamic force versus deformation behaviour of the head restraint foam.

Table 1. Rear-impact pulses used in the optimisation of the forward-facing front seat.

Crash Pulse	a_{peak} [g]	Delta-V [km/h]	a_{m50} [g]
SN(9.4)	11.7	9.4	4.72
SN(13)	11.2	13	5.97
SN(16)	10	16	7.30
SN(20)	10.63	20	7.69
TR(24)	7.5	24	7.50

2.2. Assessment of the Performance of the Forward-Facing Front Seat

The assessment criteria specified by EuroNCAP [30] are used to assess whiplash risk. As shown in Table 2, EuroNCAP specifies these criteria only for the two rear-impact crash pulses SN(16) and TR(24). Nonetheless, the performance of the seat at other crash severities is still evaluated using the criteria specified in Table 2. EuroNCAP employs the BioRID dummy to evaluate car seats by conducting sled tests; the readings obtained from the sensors of the dummy are compared with these assessment criteria. The BioRID dummy represents the 50th percentile male [5,30]. The human-body model used in this study is also the 50th percentile male and is more biofidelic than the BioRID dummy, as demonstrated in reference [15]. It should be noted that the mechanisms causing whiplash-associated disorders are not well understood since it is often not possible to objectively detect any structural injury to the neck [9]. For this reason, the EuroNCAP rating can only indicate relative injury risk and thus can only assess the relative performance of seats. Different human-body models can exhibit some variations in responses under the same test conditions [12] but the validated biofidelic human-body model used in this study can be reliably used to compare and optimise the performance of different seats. In the literature, the EuroNCAP whiplash assessment criteria [30] form the only set of reference values that can be used to rate seats; therefore, this set of EuroNCAP criteria is also used in the design of seats using the human-body model employed in this study.

Some criteria have higher performance limit (HL) and lower performance limit (LL) values for seat performance. Capping limits (CL) are applied for the other criteria. Generally, when a capping limit for a criterion is exceeded, all points from the test corresponding to that crash pulse are lost. The capping limit signals an unacceptably high risk of whiplash [30].

The criteria in Table 2 include head restraint contact time (HrCt), largest acceleration of the first thoracic vertebra T1 (T1a), largest moment at the lower neck (M_{yL}), largest shear force at the lower neck (F_{shL}), largest moment at the upper neck (M_{yU}), largest tension force at the upper neck (F_{tn}), largest negative shear force at the upper neck (F_{sh}^{-}), largest positive shear force at the upper neck (F_{sh}^{+}), head rebound velocity (v_r), neck injury criterion (NIC) and N_{km}. The injury criterion N_{km} evaluates the effects of both shear force and moment on

the upper neck. NIC is used to monitor spinal pressure gradients as a result of S-shape-like distortion in the neck, which occurs due to head retraction with respect to the upper torso. v_r corresponds to the largest resultant velocity of the head with respect to the floor of the car during which the head rebounds from the head restraint and travels toward the front of the car [30].

Table 2. EuroNCAP whiplash assessment criteria [30].

		Medium Severity Crash Pulse SN(16)			High Severity Crash Pulse TR(24)		
Criterion	**Unit**	**HL**	**LL**	**CL**	**HL**	**LL**	**CL**
NIC	m^2/s^2	11	24	27	13	23	25.5
N_{km}	-	-	-	0.69	-	-	0.75
v_r	m/s	-	-	5.2	-	-	6
F_{sh}^{+}	N	30	190	290	30	210	364
F_{sh}^{-}	N	-	-	360	-	-	360
F_{tn}	N	360	750	900	470	770	1024
M_{yU}	Nm	-	-	30	-	-	30
F_{shL}	N	-	-	360	-	-	360
M_{yL}	Nm	-	-	30	-	-	30
T1a	g	-	-	15.55	-	-	17.8
HrCt	ms	-	-	92	-	-	92

The forward-facing front seat is subjected to the rear-impact crash pulses given in Table 1 and its performance is presented in Table 3. Apart from the whiplash assessment criteria applied by EuroNCAP, Table 3 includes a seat design parameter (or tool) called Neck Distortion Index (NDI) given by Equation (1). NDI was first introduced in reference [31] but is explained again in this paper for completeness. NDI quantifies the largest amounts of protraction-type and retraction-type distortions in the neck. Protraction and retraction of the neck correspond to anterior and posterior translation-like movements of the head with respect to the upper torso, respectively. In the NDI formula, $\theta_{OC/C1}$ represents the intervertebral rotation between the base of the skull (OC) and the 1st cervical vertebra (C1), whereas $\theta_{C7/T1}$ represents the intervertebral rotation between the 7th cervical vertebra (C7) and the 1st thoracic vertebra (T1).

$$\text{NDI} = -\theta_{OC/C1} + \theta_{C7/T1} \tag{1}$$

Table 3. Performance of the forward-facing anti-whiplash front seat.

Pulse	**NIC**	N_{km}	v_r	F_{sh}^{+}	F_{sh}^{-}	F_{tn}	M_{yU}	F_{shL}	M_{yL}	**T1a**	**HrCt**	$\text{NDI}^{(-)}$	$\text{NDI}^{(+)}$
SN(9.4)	8.14	0.11	1.35	16	49	110	6.57	143	5.20	6.21	62	0.32	1.58
SN(13)	8.89	0.26	1.23	32	98	112	8.56	161	4.17	7.44	47	0.63	2.18
SN(16)	11.4	0.19	1.27	24	94	192	7.85	161	6.31	8.32	56	1.22	1.44
SN(20)	11.9	0.32	1.35	14	134	178	7.10	126	6.28	8.32	58	1.13	0.31
TR(24)	11.3	0.43	1.17	19	151	101	11.7	104	5.71	7.64	51	3.37	0.30

When evaluating seat performance, the largest NDI value (in deg) is reported within the time interval starting from the onset of impact until the head leaves the head restraint in the rebound phase. The reported negative and positive NDI values signify the largest protraction-type and retraction-type distortions of the neck, respectively. $\theta_{OC/C1}$ takes positive or negative values if there is extension or flexion in the upper neck, respectively. Similarly, $\theta_{C7/T1}$ takes positive or negative values if there is extension or flexion in the lower neck, respectively. Smaller NDI values are desired to limit the motion of the head with respect to the upper torso.

The human model in this study was previously used to model and simulate volunteer (50th percentile male) rear-impact tests [15,17] with 9.3 km/h of delta-V, where a completely

rigid seat without any head restraint was used. In these volunteer simulations, when the head fully retracted with respect to the upper torso, the most prominent retraction-type distortion (S-shape-like distortion) in the neck developed, and at this instant the NDI value was +4.5 deg. It must be stressed that this largest positive NDI value (+4.5 deg) should not be regarded as a threshold value for the development of whiplash risk because the orientation of cervical vertebrae in other real-world rear-end collisions will not be exactly the same as those of the volunteers. Although at the moment there is no clear injury assessment reference value for NDI, it is greatly helpful in optimising seat performance.

In optimising the performance of the seat using trial-and-error and engineering judgement, the upper neck shear force and the Neck Distortion Index (NDI) values are minimised. Apart from this, head restraint contact time (HrCt) is kept as low as possible, with an initial backset of 5.8 cm. The rotation of the seatback is kept below 32 deg in order to limit ramping of the occupant (i.e., upward motion of the occupant along the seatback) as specified in the EuroNCAP whiplash protocol [30]. The maximum backward displacement of the seat pan is also not allowed to exceed 10 cm to limit the horizontal motion of the seat. The optimisation procedure revealed that minimising upper neck shear forces and NDI values (while limiting the backward movement of seat components) also lowers the values of the remaining assessment criteria of the EuroNCAP whiplash protocol, as given in Table 2.

Based on the results given in Table 3, the forward-facing front seat is highly successful at satisfying the whiplash assessment criteria of EuroNCAP. Loading on the upper neck is successfully limited at all severities since F_{sh}^{+} and F_{tn} values are at or below the higher performance limit (HL); moreover, N_{km}, M_{yU} and F_{sh}^{-} values are well below their capping limits (CL). Furthermore, F_{shL}, M_{yL}, T1a, HrCt values and head rebound velocities are well below their capping limits at all severities, hence the loading at the lower neck is also low. The seat absorbs the crash energy effectively and the head contacts the head restraint without delay. Retraction-type distortion (S-shape-like distortion) in the neck is not significant since $NDI^{(+)}$ values are low and NIC values are very close to or below the higher performance limit. Protraction-type distortion, which is signified by $NDI^{(-)}$, is also not significant; this can be verified visually as well, as seen in Figure 5. From the onset of impact until the head leaves the head restraint, the intervertebral angles in the neck are below 49% of the flexion range-of-motion (ROM) and 9.7% of the extension ROM [15,16] at all severities.

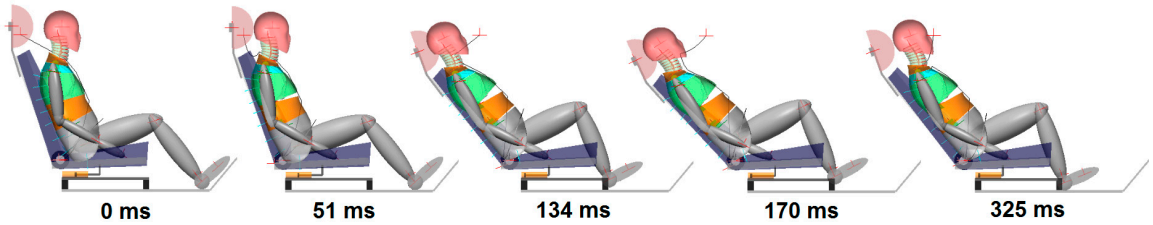

Figure 5. Seat occupant motion. The forward-facing anti-whiplash front seat is subjected to high-severity rear-impact pulse TR(24) of the EuroNCAP.

When the high-severity rear-impact crash pulse TR(24) of EuroNCAP is applied, the maximum rotation of the seatback becomes 25.2 deg and the maximum backward displacement of the seat pan becomes 6 cm. EuroNCAP applies a penalty to seatback rotations greater than or equal to 32 deg [30]. Consequently, the forward-facing front seat deserves to be an anti-whiplash seat and can earn maximum points from EuroNCAP's dynamic assessment test based on the assessment criteria given in Table 2.

Figure 5 shows frames from the simulation in which the high-severity rear-impact crash pulse TR(24) is applied to the seat-occupant system. The onset of impact is shown in the leftmost picture; the first time the head contacts the head restraint (HrCt) is shown in the second picture from the left; the head penetrates the head restraint maximally in the third picture from the left; maximum seatback rotation occurs at the instant shown in the second picture from the right; the head leaves the head restraint in the rightmost picture

in the rebound phase. The forward-facing anti-whiplash front seat is an improvement over previous research [9] on its performance and in terms of model complexity, including improved seatback, recliner mechanism, seatbelt and head restraint properties together with a more detailed occupant geometry [16].

3. Restraint System Design for Rear-Facing Seats

The forward-facing anti-whiplash front seat, described in Section 2, is reversed for use as a rear-facing seat and subjected to a frontal impact corresponding to a full-width rigid barrier frontal crash at an impact speed of 56 km/h. Under this condition, neck shear forces are over 600 N and the largest negative value of NDI becomes as large as −9 deg. The problem is that the foam material used in the seatback and head restraint, the recliner mechanism and the energy absorber under the seat pan cannot cope with such high-severity impacts as their resistance to impact loading is not strong enough at these severities. Thus, the seat components cannot provide enough restraint force to support the human body quickly and the human body attains high velocities with respect to the vehicle cabin. Consequently, the head and the upper torso interact violently with the head restraint and seatback, respectively, increasing the severity of injuries to the neck, head and torso as the seat components bottom out. Since this outcome is not acceptable, an improved design for rear-facing seats is proposed in this paper.

3.1. Design Principles and Modelling Details of the Rear-Facing Seat

The rear-facing seat proposed in this paper comprises a restraint system called a torso plate, as shown in Figure 6. Two torso plates (thorax torso plate and lumbar torso plate) are mounted on the upper and lower seatbacks, respectively. The torso plates, which are rigid, restrain the thoracic and lumbar spines of the human body by restricting the rearward rotation of the upper and lower torso towards the seatback during frontal impact. In order to adjust the position and orientation of the torso plates according to occupant size and posture, the plates are loosened at the pivot points P, rotated and then fixed again at points P before travel. The pivot point P can be translated along the seatback to accommodate different occupants. The torso plates can also be custom-made or made of several lockable pieces to conform to the occupant's torso. When the torso is resting against the torso plates, the head restraint must be adjusted to provide almost zero backset between the head restraint and the head in the normal sitting posture, as shown in Figure 6. The torso plates together with the head restraint restrict head/neck/torso motion with respect to the seat. The seatback angle is again set to 20 deg from vertical to be consistent with that of the forward-facing front seat. The rear-facing seat has a fixed recliner to eliminate excessive seatback rotation, especially at high-severity frontal impacts.

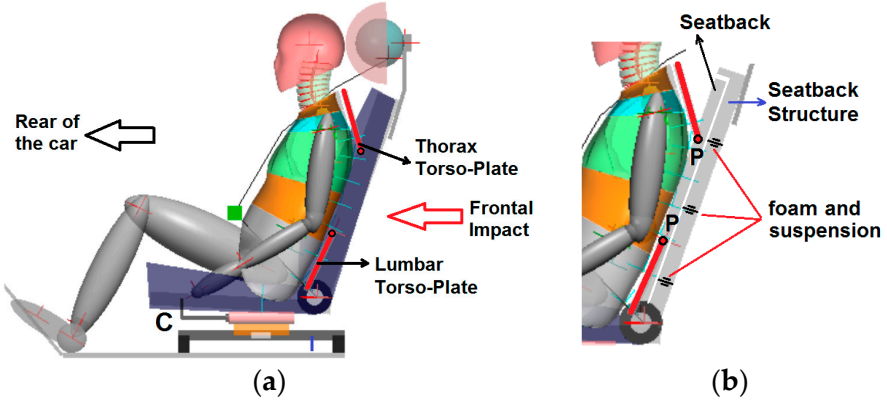

Figure 6. (**a**) Rear-facing seat and occupant just before impact in the normal sitting posture; (**b**) Detailed view of torso plates, seatback structure and seatback foam and suspension.

The seatback is a rigid plate whose front surface is covered by a foam with a thickness of 1.5 cm for comfort. There is foam and suspension in between the seatback structure

and the rear surface of the seatback that enables the seatback to displace into the seatback structure by at most 3.5 cm, as shown in Figure 6. The compliance of seatback foam and suspension is uniform throughout the seatback. Figure 7 shows the total dynamic force on the seatback versus the total deformation of seatback foam and suspension at a crash pulse with a delta-V of 64 km/h. The measurement of dynamic force and deformation is the same as that of the forward-facing seat. The seat pan foam has a thickness of 2 cm. The dynamic force versus the deformation characteristics of the seat pan foam are similar in shape to those of the forward-facing seat. The compliance of seat the pan foam is uniform throughout the seat pan. The foam of the head restraint is 3 cm in thickness. The dynamic force versus deformation characteristics of the head restraint are similar in shape to those of the forward-facing seat but the foam is firmer and produces 2250 N of force at 3 cm deformation. The compliances of head restraint foam, seatback foam and suspension and seat pan foam are tailored to limit distortion of the neck during impact.

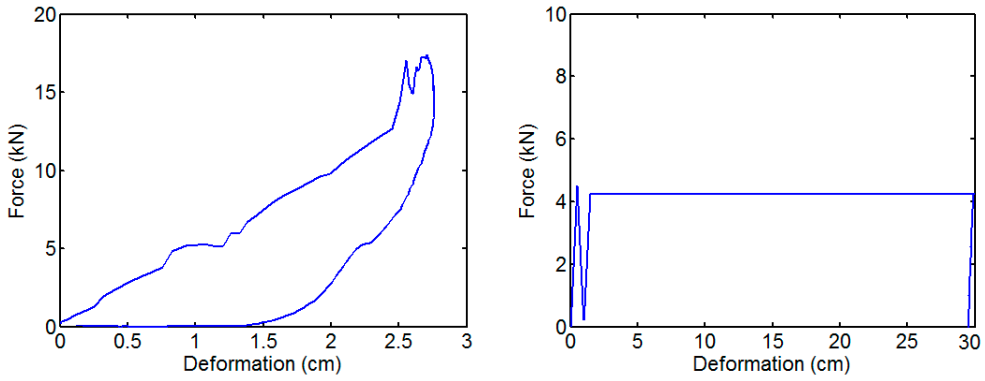

Figure 7. (**a**) Dynamic force versus deformation of seatback foam and suspension at a crash pulse with 64 km/h of delta-V; (**b**) Force versus deformation characteristics of the constant-force deformation element.

As the recliner is fixed, there is a need for an energy-absorbing device (C) underneath the seat pan, as shown in Figure 6, which is a combination of a damper (with a constant damping coefficient of 4000 kg/s) and a constant-force deformation element (with 4250 N of resistive force). In order to keep the energy-absorbing device in place during normal use, a breakaway element with a breakaway force of 4.5 kN is inserted. The force versus deformation behaviour of the constant-force deformation element is given in Figure 7. Constant-force deformation elements are commonly used in aviation [32,33] and automotive industries [34,35] to cushion the impact. The deformation element is plastically deformed and its elastic rebound is minimal; nevertheless, the energy-absorbing device applies high damping (30 kNs/m) against seat pan motion in the reverse direction (towards the rear of the car) to limit uncontrolled motion of the seat in the rebound phase of the impact during frontal crashes.

The seat features an integrated seatbelt (V4 type 4-point seatbelt) so that it can be moved in an autonomous car while providing belt support at all times. The presence of torso plates, integrated seatbelts and fixed recliners eliminates the ramping (upward displacement) of the torso along the seatback. The main advantage of the thorax torso plate is that it prevents the development of relative velocity between the upper seatback and upper torso, which improves neck and head protection and offers close support to the head by the head restraint. If the lumbar torso plate is not used together with the thorax torso plate, counter-clockwise rotation of the torso into the seatback structure develops (see Figure 6) during frontal impact, and the head is moved away from the head restraint, leading to head retraction relative to the upper torso.

In the following sections, it will be shown that in order to limit injury risk, the energy-absorbing device should provide a seat pan displacement of 27.8 cm at the highest severity

frontal impact studied in this paper. This requires sufficient space within the car interior. If there is sufficient legroom, the seat can be moved towards the rear of the car before impact using an electric motor. If the seat is moved 10 cm towards the rear of the car and then the seat displaces 30 cm towards the front of the car at the end of the impact, the net displacement (see Figure 8) of the seat towards the front of the car is reduced to 20 cm. Figure 8 shows an application in which the seat pan (SP) is moved 10 cm with respect to the car floor (CF) 2 s t before an inevitable frontal impact. At time equals −2 s, the lock pin (L) is released electromechanically and the electric motor is activated after the sensors (lidar, radar) send a signal indicating that the impact is about to happen. The lock pin (L) secures the energy-absorbing device (C) to the car floor (CF) during normal travel. A spring-loaded rectangular wedge (W) is placed between the car floor (CF) and the energy-absorbing device (C). The electric motor drives the seat pan and the energy-absorbing device on the car floor until the wedge (W) fits into the slot (S). Once the wedge is in the slot, the translation of the seat pan towards the rear of the car is complete and the electric motor is turned off. The frontal impact starts when time is equal to zero, as shown in Figure 8. It should be noted that the seat rails are fixed but the energy-absorbing device (C) moves together with the seat above the rails 2 s before impact. The aim of this mechanism is to open up space for the seat to travel, while the energy-absorbing device (C) absorbs crash energy. The seat system still works and offers exactly the same protection without the activation of this mechanism since the net seat pan displacement does not change. The presented mechanism is only a concept design and the practical application of sensors can be the subject of another project. This mechanism is intended for use in future autonomous cars.

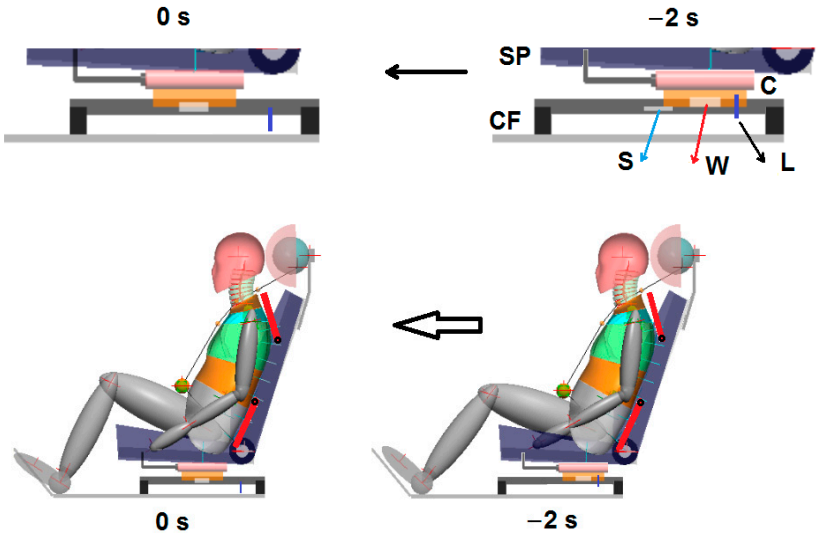

Figure 8. The translation of the rear-facing seat towards the rear of the car 2 s before frontal impact. Frontal impact starts at 0 s. The top figure shows a detailed view of the mechanism under the seat pan.

During the translation of the seat towards the rear of the car, there is no significant change in the posture of the head/neck/torso since the peak acceleration of the seat provided by the electric motor is only 0.02 g (it should be noted that an average car, when driven in the first gear, has an acceleration of 0.5 g [36]).

The car floor structure (CF) and the energy-absorbing device (C) are produced and assembled in pairs. In other words, there are two CF and two energy-absorbing devices (C) located on both sides of the seat, similar to seat rails that are also located on both sides of the seat pan. Therefore, the feet do not contact CF and C during the simulations, because there is space between the two CF and the two energy-absorbing devices (C). The feet rise slightly above the floor as the legs retract during impact.

3.2. Performance of the Rear-Facing Seat

In the United States NCAP crash tests, cars impact a fixed rigid wall frontally with 100% overlap at impact speeds of 40 km/h and 56 km/h [6]. These tests are called full-width rigid barrier (FWRB) frontal impact tests. In order to assess the performance of the rear-facing seat, frontal-impact crash pulses from FWRB tests are used together with the rear-impact crash pulses given in Table 3 considering that the rear-facing seat can also be reversed to be used as forward-facing. However, crash test reports and sensor data in the US NCAP FWRB crash tests involve only the horizontal and vertical components of occupant compartment acceleration but do not report any data on car rotation in the form of pitching motion. In FWRB frontal impact tests, the pitching motion becomes discernible starting from an impact speed of 40 km/h [6]. Therefore, a detailed finite element (FE) model of the 2010 Toyota Yaris model, which can be downloaded from the National Highway Traffic Safety Administration (NHTSA) website [6], was subjected to FWRB frontal impact tests at 40 km/h and 56 km/h impact speeds using ANSYS Mechanical APDL and LS-DYNA solver as shown in Figure 9. The FE model of the Toyota Yaris was built and validated by the National Crash Analysis Centre (NCAC) of George Washington University [37]. The translational and angular accelerations around the right rear seat (RS) on the car floor along the positive x, z and y axes, respectively, of the inertial frame are extracted from the FE simulations as shown in Figures 9 and 10. The accelerations on the car floor (at RS) are filtered according to the Society of Automotive Engineers (SAE) Recommended Practice J211-1 [38].

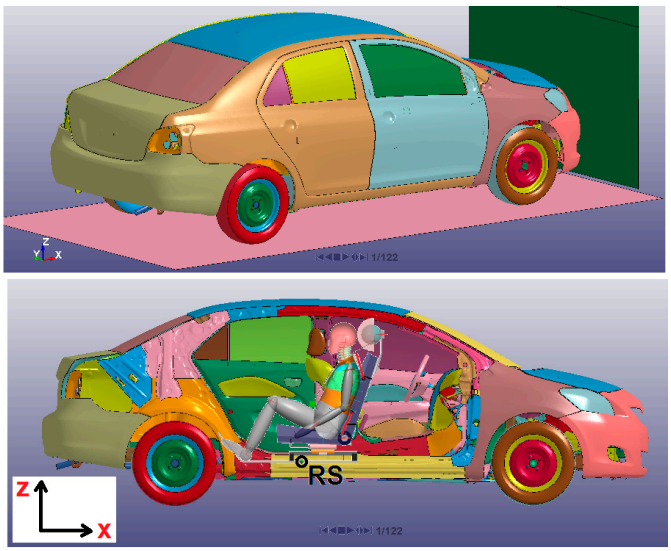

Figure 9. The Toyota Yaris FE model together with the human model in the normal sitting posture just before FWRB frontal impact (time: 0 s). The rigid barrier (wall) is shown in green.

Table 4. Higher-severity crash pulses used in the optimisation of the rear-facing seat.

Crash Pulse	a_{peak}	Delta-V	a_{m50}
HS(35)	16 g (x)	35 km/h (x)	10.54 g (x)
NC(47)	−27.3 g (x)	−47.5 km/h (x)	−20.7 g (x)
	8.61 g (z)	−1.93 km/h (z)	−1.68 g (z)
	3.72 deg/s^2 (y)	−2.36 deg/s (y)	−570 deg/s^2 (y)
NC(64)	−46.56 g (x)	−64.2 km/h (x)	−31.92 g (x)
	12.89 g (z)	−4.98 km/h (z)	3.26 g (z)
	13,096 deg/s^2 (y)	−12.87 deg/s (y)	2963 deg/s^2 (y)

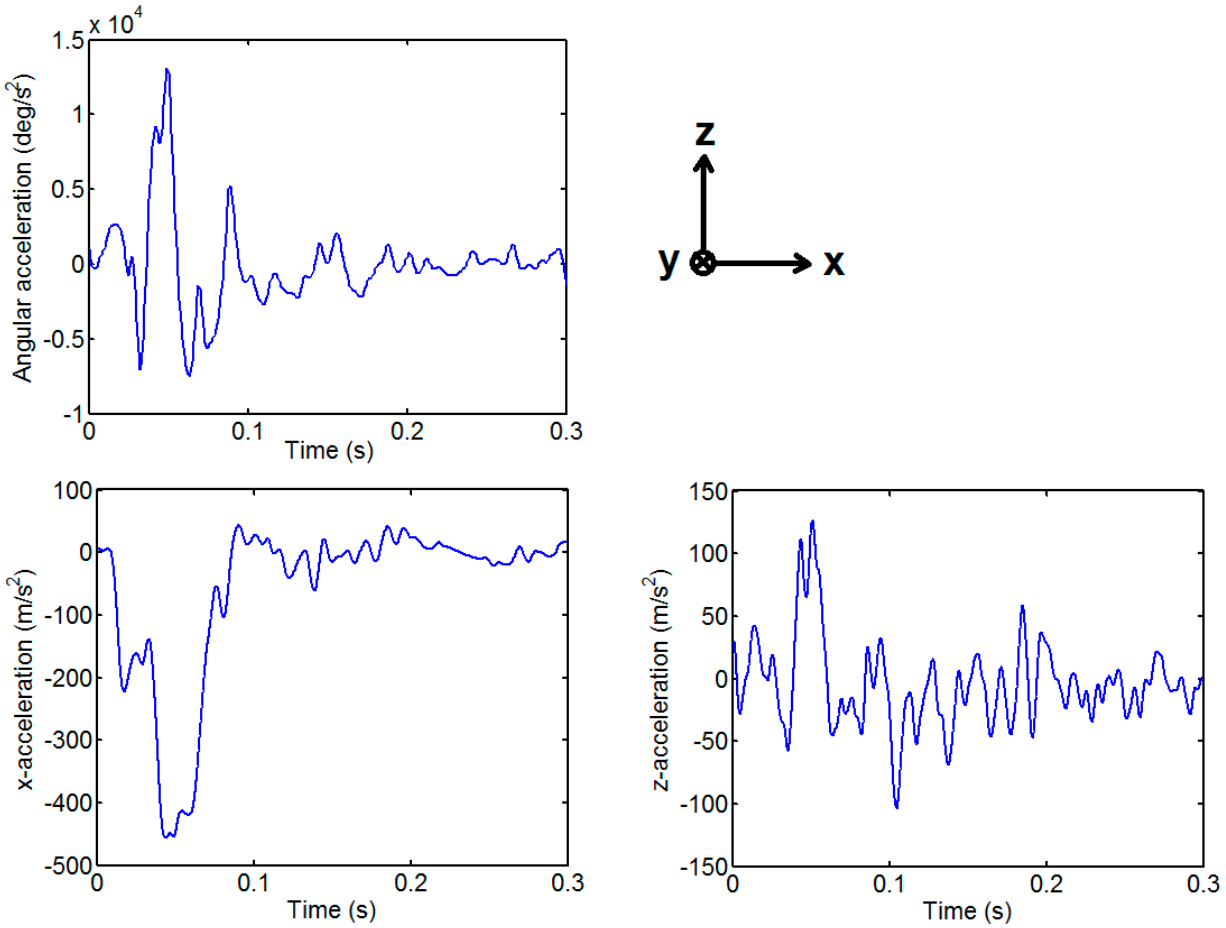

Figure 10. The angular and translational accelerations around the right rear seat (RS) on the car floor when the car experiences an FWRB frontal impact at an impact speed of 56 km/h. The presented accelerations correspond to the crash pulse NC(64) in Table 4.

Table 4 presents the crash pulses used in the optimisation of the rear-facing seat. The frontal-impact crash pulses NC(47) and NC(64) are obtained from the FE simulations of the Toyota Yaris. The crash pulses NC(47) and NC(64) develop when the car impacts the rigid wall at impact speeds of 40 km/h and 56 km/h, respectively. The crash pulse HS(35) is originally a very high-severity rear-impact crash pulse corresponding to the Federal Motor Vehicle Safety Standards 301 (FMVSS301) moving barrier rear-impact crash tests designed to check fuel system integrity [24]. Although HS(35) is a rear impact pulse, it is still applied to the seat considering that the proposed rear-facing seat with torso plates can be reversed to be used as a forward-facing seat. The crash pulse HS(35) is applied horizontally to the proposed rear-facing seat. Table 4 includes changes in velocities (delta-V), means and peak accelerations of the crash pulses along the x, y, and z axes of the inertial frame. Figure 11 shows that the rear of the car ascends and then descends, hence the delta-V in the z direction is negative for an impact duration of 0.3 s.

3.2.1. Performance of the Rear-Facing Seat at Lower Severities

The proposed rear-facing seat with torso plates is specifically designed to offer protection at higher severities but its performance should be checked at lower severities as well. For this purpose, the proposed rear-facing seat with torso plates is reversed to be used as a forward-facing seat and the rear-impact crash pulses given in Table 1 are applied to evaluate its performance using the EuroNCAP whiplash assessment criteria, as shown in Table 5. It can also be assumed that the rear-impact crash pulses in Table 1 can be treated as if they were frontal-impact crash pulses to be applied to the proposed rear-facing seat.

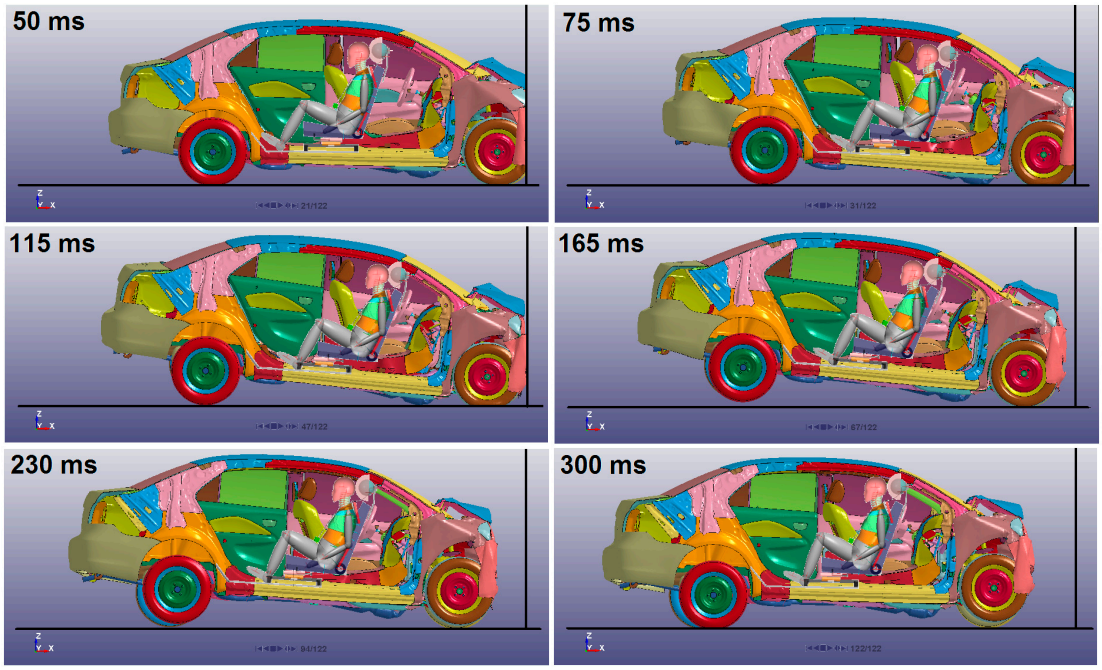

Figure 11. Car, rear-facing seat and occupant motion. FWRB impact at an impact speed of 56 km/h producing the crash pulse NC(64). The occupant has the normal sitting posture before impact. In this figure, the frames from the multi-body seat occupant simulation are superimposed on the frames from the FE simulation of the FWRB car impact.

Table 5. Performance of the proposed seat (with torso plates) at lower severities. The occupant is in the normal sitting posture.

Pulse	NIC	N_{km}	v_r	F_{sh}^{+}	F_{sh}^{-}	F_{tn}	M_{yU}	F_{shL}	M_{yL}	T1a	HrCt	$NDI^{(-)}$	$NDI^{(+)}$
SN(9.4)	7.79	0.17	0.49	17.5	88	49	2.57	84	4.01	7.87	14	2.29	0.28
SN(13)	11.3	0.26	0.47	17.7	135	81	3.28	129	3.64	12.0	8	1.21	0.17
SN(16)	13.3	0.25	0.46	15.7	130	97	6.08	125	3.55	8.87	16	2.57	0.29
SN(20)	9.19	0.21	0.41	12.8	115	17	3.56	106	3.70	7.74	11	2.79	0.22
TR(24)	15.2	0.23	0.42	9.38	128	85	3.42	114	3.64	8.25	11	2.14	0.21

Table 5 indicates that when the occupant is in the normal sitting posture at lower severities, the upper neck loading is low since the N_{km}, F_{sh}^{-}, M_{yU} values are well below their capping limits (CL) of 0.75, 360 N and 30 Nm, respectively. Moreover, F_{sh}^{+} and F_{tn} values are below their higher performance limits (HL), which are 30 N and 470 N, respectively. The loading on the lower neck is also low, as indicated by F_{shL} and M_{yL} values, which are well below their capping limits of 360 N and 30 Nm, respectively. Since the head restraint provides close support for the head, head restraint contact times are minimal in comparison to the capping limit of 92 ms. The energy-absorbing device (C) underneath the seat pan provides sufficient energy absorption (in spite of the fixed recliner) and is able to limit upper torso accelerations (T1a), which are lower than the capping limit of 17.8 g. Since a fixed recliner is used, the elastic rebound in the system is not significant, hence head rebound velocities (v_r) are well below the capping limit of 6 m/s. Head retraction relative to the upper torso is not significant as $NDI^{(+)}$ values are very low and NIC values are slightly above but close to the higher performance limits of the crash pulses SN(16) and TR(24). From the onset of impact until the head leaves the head restraint, the intervertebral angles in the neck are below 19% of the flexion range-of-motion (ROM) and 15% of the extension ROM; consequently, head protraction with respect to the upper torso is also low, as exemplified by the $NDI^{(-)}$ values. At crash pulse TR(24), the seat pan displaces by an amount of 6.3 cm at most after the impact begins at 0 s.

3.2.2. Performance of the Rear-Facing Seat at Higher Severities

Whiplash is usually categorised as a minor injury, which is graded as AIS1 in the Abbreviated Injury Scale (AIS) [39]. The mechanisms causing whiplash-associated disorders are not completely understood since it is often not possible to objectively diagnose any structural injury to the neck [39]. For this reason, it is not easy to establish injury probability curves for whiplash and EuroNCAP employs only a sliding scale system [30] based on higher and lower performance limits, together with a capping limit to score seat performance as shown in Table 2. The proposed rear-facing seat will be subjected to higher severity frontal impacts; therefore, regions other than the neck of the human body have to be monitored as well. At these higher severities, AIS2+ (AIS $\geq$ 2) type injuries will be of concern. AIS2-type injury refers to a moderate level of injury [39]. The injury criteria and the relevant injury assessment reference values (IARVs) for higher severity impacts are given in Table 6. These IARVs are in general approximate threshold values for AIS2+ type injuries [39–46]. The IARVs in Table 6 apply to the 50th percentile male human, who is the occupant model used in this paper. These IARVs are also used for the 50th percentile male frontal impact dummy, which is the Hybrid III dummy positioned in a forward-facing seat.

Table 6. Injury assessment reference values (IARVs) for higher severity impacts.

Region	Criterion	IARV	Reference
Head	HIC_{15}	700	[41]
	BrIC	-	[40]
Upper Neck	F^{+}_{shU} (+shear)	3100 N	[11,39]
	F^{-}_{shU} (−shear)	3100 N	[11,39]
	F_{tnU} (tension)	3300 N	[39,41]
	F_{cmU} (compr.)	4000 N	[39,41]
	M_{yUE} (extension)	57 Nm	[39,41]
	M_{yUF} (flexion)	190 Nm	[39,41]
	N_{ij}	1	[39,41]
Lower Neck	F^{+}_{shL} (+shear)	3100 N	[11,39]
	F^{-}_{shL} (−shear)	3100 N	[11,39]
	F_{tnL} (tension)	3300 N	[39,41]
	F_{cmL} (compr.)	4000 N	[39,41]
	M_{yLE} (extension)	194 Nm	[11]
	M_{yLF} (flexion)	380 Nm	[11]
Thorax	Ta_3 (thorax acc.)	60 g	[39,41]
	cd (chest defl.)	42 mm	[30,39]
	VC	1 m/s	[39,44,45]
Lumbar Spine	L_{tn} (tension)	12.2 kN	[11]
	L_{cm} (compr.)	6400 N	[11,39]
Hip	H_{cm} (axial compr.)	10 kN	[39,42]
Femur (thigh)	F_{cm} (axial compr.)	10 kN	[30,42,43]
Tibia	T_{cm} (axial compr.)	8 kN	[30,39,43]
Tibia	TI	1.3	[30,39,43,46]

As shown in Table 6, two criteria are applied for the head region. The Head Injury Criterion (HIC_{15}) is based on the resultant acceleration of the head centre of gravity calculated over a 15 ms moving time interval. The IARV for HIC_{15} is 700, which corresponds to a 31% probability of AIS2+ skull fracture [41]. The Brain Injury Criterion (BrIC) is based on the angular velocity of the head and there is no established IARV for this criterion but AIS1- and AIS2-type injury probabilities (based on maximum principal strain) are calculated in this paper using the published injury risk curves [40].

There are seven injury criteria comprising shear, tension, compression forces, extension/flexion moments and N_{ij} at the upper neck, which correspond to the joint between the base of the skull and the 1st cervical vertebra. Positive shear force develops when the

head moves rearward with respect to the upper torso in a typical retraction-type distortion in the neck [5]. Extension and flexion moments develop when the neck bends rearward and forward, respectively [39,41]. N_{ij} is a neck injury criterion that employs a combination of upper neck axial forces and extension/flexion moments. The IARV for N_{ij} is 1, which corresponds to a 30% probability of AIS2+ type injury [41]. Dislocation in the neck without fracture is an AIS2-type injury [39]. Similarly, there are six injury criteria for the loading at the lower neck acting at the joint between the 7th cervical vertebra and the 1st thoracic vertebra.

The criteria for thorax (chest) injuries include 3 ms clip thorax acceleration (Ta_3), maximum chest deflection (cd) and Viscous Criterion (VC). The IARVs for Ta_3 and cd are 60 g and 42 mm, which correspond to 90% and 50% probabilities of AIS2+ injury, respectively [41]. AIS2-type thorax injuries include bronchus tear, pneumothorax, sternum fractures and two rib fractures [39]. VC takes into account the rate-dependent injury mechanism in the thorax and can predict severe thoracic injuries (AIS4+) in a blunt impact [44]. The IARV for VC is 1 m/s and this corresponds to 80% and 25% probabilities of AIS2+ and AIS4+ type injuries, respectively [44,45]. The IARVs for the lumbar spine comprise tension and compression forces in the lumbar spine. At an IARV of 6400 N, the probability of lumbar spine fracture due to compression is reported as 100% [47].

Pelvis and lower extremity injuries are assessed using four established criteria for frontal impacts for the standard automotive posture in forward-facing seats, which include hip, femur, tibia axial compression forces and Tibia Index (TI). The IARV for H_{cm} is 10 kN, which corresponds to the hip fracture and dislocation force in the standard automotive posture, causing a 100% probability of AIS2+ type injury [39,42]. The IARV for F_{cm} is 10 kN, which causes patellar and femur fractures/dislocations and produces a 35% probability of AIS2+ injury [43]. The IARV for T_{cm} is 8 kN, which causes a 71% probability of AIS2+ type injury comprising tibial plateau or condyle injury [43]. TI predicts tibia shaft fracture by utilising the bending moment and compression force at the upper and lower end of each tibia [39,43,46]. The IARV for TI is 1.3, which corresponds to approximately 56% probability of AIS2+ injury of the tibia shaft [43].

Tables 7–13 present the performance of the rear-facing seat (with the occupant in the normal sitting posture) by indicating the values of the injury criteria for each region of the human body at higher severities. In these Tables, the responses of the occupant model are given and for each response, the corresponding percentages of IARV and percentage probability of injury are given in parentheses where available.

Table 7. Rear-facing seat performance (normal sitting posture) at higher severities (head).

Pulse	HIC_{15}	BrIC
HS(35)	6.86 (1% IARV) (0% AIS2+)	0.03 (3% AIS1, 0% AIS2)
NC(47)	39.3 (6% IARV) (0% AIS2+)	0.04 (4% AIS1, 0% AIS2)
NC(64)	89.6 (13% IARV) (0% AIS2+)	0.042 (5% AIS1, 0% AIS2)

Table 8. Rear-facing seat performance (normal sitting posture) at higher severities (upper neck).

Pulse	N_{km}	F^{+}_{shU}	F^{-}_{shU}	F_{tnU}	F_{cmU}	M_{yUE}	M_{yUF}	N_{ij}
HS(35)	0.29 (29% IARV)	15.5 (0.5% IARV)	157 (5% IARV)	76.2 (2% IARV)	445 (11% IARV)	4.74 (8% IARV)	0.66 (0.3% IARV)	0.12 (13% AIS2+) (12% IARV)
NC(47)	0.42 (42% IARV)	13.1 (0.4% IARV)	219 (7% IARV)	223 (7% IARV)	634 (16% IARV)	7.37 (13% IARV)	1.54 (0.8% IARV)	0.15 (13% AIS2+) (15% IARV)
NC(64)	0.67 (67% IARV)	11.6 (0.4% IARV)	350 (11% IARV)	445 (13% IARV)	729 (18% IARV)	10.7 (19% IARV)	5.52 (3% IARV)	0.19 (14% AIS2+) (19% IARV)

Table 9. Rear-facing seat performance (normal sitting posture) at higher severities (lower neck).

Pulse	F^{+}_{shL}	F^{-}_{shL}	F_{tnL}	F_{cmL}	M_{yLE}	M_{yLF}
HS(35)	75 (2.4% IARV)	145 (5% IARV)	99 (3% IARV)	420 (11% IARV)	3.09 (1.6% IARV)	4.41 (1% IARV)
NC(47)	124 (4% IARV)	133 (4.3% IARV)	125 (4% IARV)	721 (18% IARV)	5.02 (2.6% IARV)	5.09 (1.3% IARV)
NC(64)	309 (10% IARV)	149 (4.8% IARV)	179 (5.4% IARV)	837 (21% IARV)	14.0 (7.2% IARV)	5.92 (1.6% IARV)

Table 10. Rear-facing seat performance (normal sitting posture) at higher severities (overall neck).

Pulse	v_r	NIC	$NDI^{(-)}$	$NDI^{(+)}$
HS(35)	0.43 (7% IARV)	16.8 (62% IARV)	3.48	0.14
NC(47)	0.54 (9% IARV)	10.6 (39% IARV)	3.49	0.29
NC(64)	0.87 (14% IARV)	19.7 (73% IARV)	2.74	0.96

Table 11. Rear-facing seat performance (normal sitting posture) at higher severities (thorax).

Pulse	Ta_3	cd	VC
HS(35)	11.9 (20% IARV) (36% AIS2+)	2.3 (5.5% IARV) (14% AIS2+)	0.0072 (0.72% IARV) (0% AIS2+)
NC(47)	25.2 (42% IARV) (55% AIS2+)	2.6 (6.2% IARV) (14% AIS2+)	0.005 (0.5% IARV) (0% AIS2+)
NC(64)	32.6 (54% IARV) (65% AIS2+)	3.2 (7.6% IARV) (15% AIS2+)	0.006 (0.6% IARV) (0% AIS2+)

Table 12. Rear-facing seat performance (normal sitting posture) at higher severities (lumbar spine).

Pulse	L_{tn}	L_{cm}
HS(35)	0	2172 (34% IARV)
NC(47)	0	2826 (44% IARV)
NC(64)	0	3512 (55% IARV)

Table 13. Rear-facing seat performance (normal sitting posture) at higher severities (hip–femur–tibia).

Pulse	H_{cm}	F_{cm}	T_{cm}	TI
HS(35)	1.3 (13% IARV) (0% AIS2+)	0.21 (2.1% IARV) (0% AIS2+)	43 N (0.54% IARV) (0% AIS2+)	0.063 (4.8% IARV) (0% AIS2+)
NC(47)	2.18 (21.8% IARV) (0% AIS2+)	0.42 (4.2% IARV) (0% AIS2+)	45 N (0.56% IARV) (0% AIS2+)	0.11 (8.5% IARV) (0% AIS2+)
NC(64)	3.2 (32% IARV) (0% AIS2+)	0.50 (5% IARV) (0% AIS2+)	44 N (0.55% IARV) (0% AIS2+)	0.13 (10% IARV) (0% AIS2+)

To check for AIS1-type whiplash-associated disorders and to compare the performance of the rear-facing seat at higher severities with that of the forward-facing seat at lower severities, the values of the injury criteria N_{km}, NIC and v_r are also reported in Tables 8 and 10.

The AIS1 injury threshold for N_{km} is 1, which is used as the corresponding IARV [39]. For head rebound velocity v_r, the EuroNCAP capping limit of 6 m/s is regarded as the IARV. For NIC, the EuroNCAP capping limit of 27 m^2/s^2 is used as the IARV. As indicated by the NDI values in Tables 5 and 10, protraction-type distortion in the neck is more dominant than retraction-type distortion, hence the NIC limit for protraction-type distortion is 25 m^2/s^2, which corresponds to a 50% probability of AIS1-type whiplash-associated disorders [48].

Figure 12 shows the rear-facing seat and human model motion when they are subjected to crash pulse NC(64), which is the highest severity pulse applied in this study. The crash simulation is composed of two stages. In the first stage, the FE simulation in which the car impacts the rigid wall without the rear-facing seat and the human model is run. The FE simulation is used to record the crash pulse around the right rear seat (RS) on the car floor. In the second stage, the recorded crash pulse is applied to point RS under the seat to run the seat-occupant simulation similar to the EuroNCAP dynamic whiplash sled tests [5]. Another reason behind this two-stage simulation procedure is that Visual Nastran (seat-occupant model) and LS-Dyna (car model) cannot be co-simulated. Nevertheless, this two-stage simulation procedure has the potential to reduce computation time. The FE seat model that comes with the Toyota Yaris FE model is not used, instead, the multi-body seat model built in Visual Nastran is used in the seat-occupant simulation, which is separate from the FE simulation.

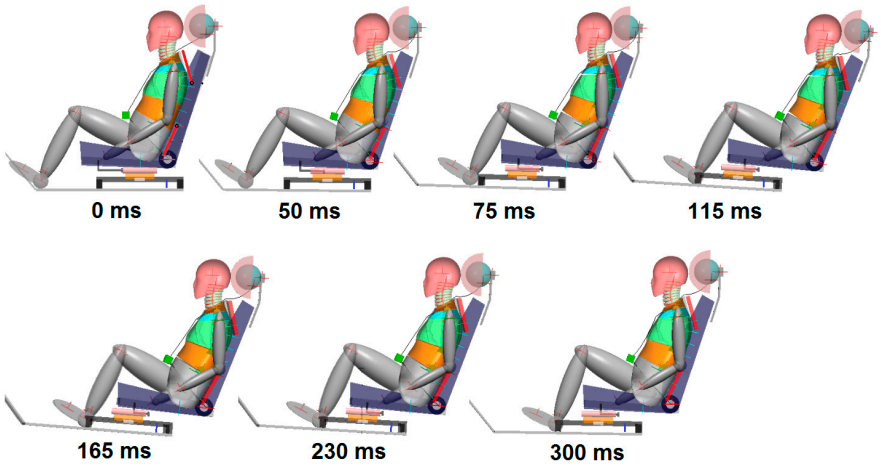

Figure 12. Rear-facing seat and occupant motion. The seat-occupant system experiences a FWRB frontal crash at an impact speed of 56 km/h (crash pulse NC(64)). The occupant has the normal sitting posture before impact.

As shown in Figures 9 and 11, the predominant motion of the car during impact consists of translations along the x and z axes and rotations around the y-axis. Therefore, the recorded crash pulse (shown in Figure 10) representing this predominant motion of the car is applied to point RS under the seat. The seat-occupant motion happens in the sagittal plane, as shown in Figure 12. This is a reasonable approximation that is commonly applied in sled tests to test and design restraint systems.

In Figure 12, the largest protraction-type distortion in the neck occurs at 50 ms; the largest retraction-type distortion in the neck occurs at 75 ms, and at this instant seatback foam and suspension deformation reach maximum levels. The largest car rotation (around 5 deg) occurs at 165 ms and the car lands on the road at 300 ms (see Figure 11 as well). The human-body model rebounds from the seatback after 300 ms.

3.2.3. Performance of the Rear-Facing Seat with Out-of-Position Occupant

In this section, a potential worst-case scenario is investigated in which the out-of-position occupant is leaning forward before a high-severity FWRB frontal impact. This scenario is shown in Figures 13 and 14; the occupant is out-of-position 750 ms before the impact such that the shortest distance between the head restraint and the head is 10 cm.

The velocity of the car is 70.8 km/h when hard braking is applied 750 ms before the impact. The braking profile, which is a typical one [49,50], is shown in Figure 13. Here, the time to reach 0.8 g deceleration is 450 ms. Braking continues for 750 ms until the car impacts the rigid wall with a velocity of 56 km/h at 0 ms. Due to braking, the head and upper torso acquire a relative velocity with respect to the thorax torso plate and head restraint. This scenario is designed to evaluate the loading and distortion in the neck when the head and upper torso interact with the head restraint and the thorax torso plate.

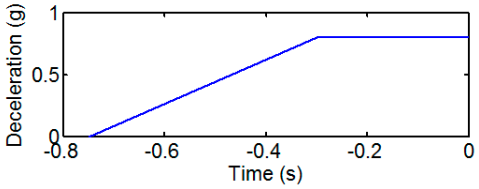

Figure 13. The braking profile of the car before it impacts the rigid wall at 0 s.

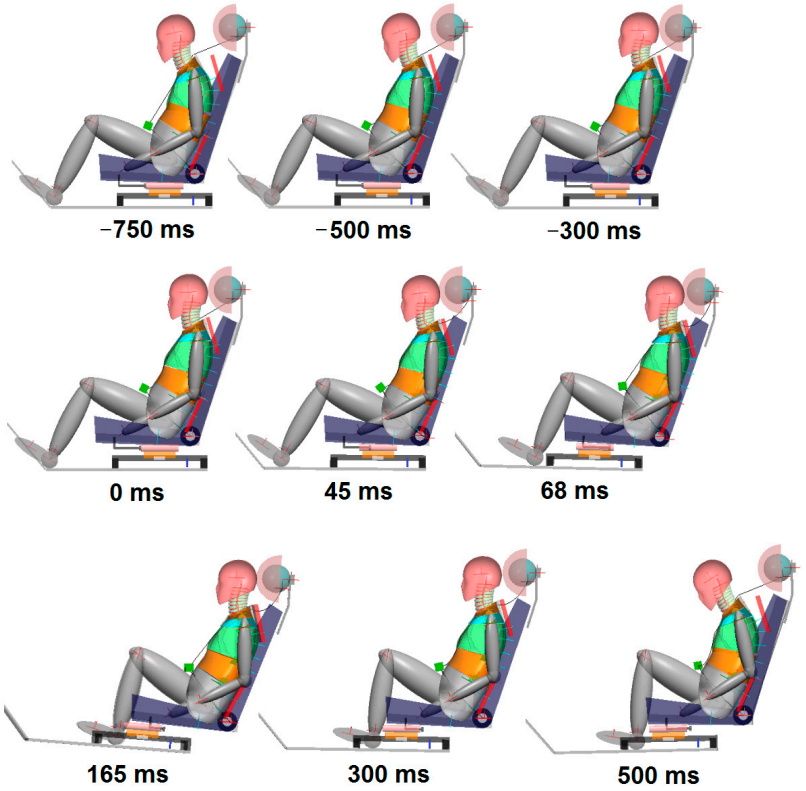

Figure 14. Rear-facing seat (with harder head restraint) and occupant motion. The occupant is leaning forward before the crash. The FWRB frontal impact starting at 0 ms is preceded by braking. The seat-occupant system experiences crash pulse NC(64).

The torso of the human-body model [15,16] used in this study is multi-segmented and composed of five parts that are connected to each other using four revolute joints with nonlinear springs and dampers. These joints are situated at the anatomical locations of T3 (3rd thoracic vertebra), T5 (5th thoracic vertebra), T11/T12 (at the intersection of the 11th and 12th thoracic vertebrae) and L3/L4 (at the intersection of the 3rd and 4th lumbar vertebrae). The idea of simplifying the spine model using fewer joints than that of the actual human body is also used in the most recent state-of-the-art rear-impact dummy prototype called SETs [51]. To set the human-body model out of position, the T11/T12 joint is flexed (rotated forward) without exceeding its range of motion.

Figure 14 shows the rear-facing seat and the out-of-position occupant motion in which the largest protraction-type distortion in the neck occurs at 45 ms; the largest retraction-type

distortion in the neck occurs at 68 ms; the largest car rotation (around 5 deg) occurs at 165 ms and the car lands on the road at 300 ms.

Table 14 shows the performance of the rear-facing seat (with the occupant leaning forward) when subjected to crash pulse NC(64). It can be seen that in this scenario, neck and tibia loadings are increased in comparison to the case where the occupant has the normal sitting posture prior to impact. The rear-facing seat originally has a head restraint producing a total dynamic force of 2250 N on the head form impactor at 3 cm deformation before it bottoms out; however, in this scenario, retraction-type distortion in the neck is increased ($NDI^{(+)}$ being 3.88 deg). To counteract this, a harder head restraint, which produces a total dynamic force of 2650 N on the head form impactor at 2.5 cm deformation before it bottoms out, is installed. The responses with the harder head restraint are shown in parentheses in Table 14. With the harder head restraint, the retraction-type distortion in the neck is significantly reduced while the protraction-type distortion in the neck is significantly limited.

Table 14. Performance of the rear-facing seat in crash pulse NC(64) (occupant leaning forward). Responses with the harder head restraint are shown in parentheses. The symbol (-) indicates that the corresponding data is not available.

Region	Criterion	Value	% IARV	% AIS
Head	HIC_{15}	105 (117)	15% (17%)	0% (0%) AIS2+
	BrIC	0.068 (0.070)	-	18% (19%) AIS1
Upper Neck	N_{km}	0.84 (0.83)	84% (83%)	-
	F^{+}_{shU}	41 (100) N	1.3% (3.2%)	-
	F^{-}_{shU}	416 (434)N	13% (14%)	-
	F_{tnU}	435 (334) N	13% (10%)	-
	F_{cmU}	782 (760) N	20% (19%)	-
	M_{yUE}	13.5 (17.7) Nm	23% (31%)	-
	M_{yUF}	9.15 (13.5) Nm	4.8% (7.1%)	-
	N_{ij}	0.20 (0.24)	20% (24%)	14% (15%) AIS2+
Lower Neck	F^{+}_{shL}	265 (194) N	8.5% (6.3%)	-
	F^{-}_{shL}	175 (179) N	5.6% (5.8%)	-
	F_{tnL}	205 (217) N	6.2% (6.6%)	-
	F_{cmL}	899 (891) N	22% (22%)	-
	M_{yLE}	11.5 (15.5) Nm	5.9% (8%)	-
	M_{yLF}	9.76 (10.7) Nm	2.6% (2.8%)	-
Overall Neck	v_r	0.88 (0.89) m/s	14.7% (14.8%)	-
	NIC	26 (32) m^2/s^2	96% (118%)	50% (70%) AIS1
	$NDI^{(-)}$	0.27 (2.75) deg	-	-
	$NDI^{(+)}$	3.88 (0.90) deg	-	-
Thorax	Ta_3	32.6 (32.6) g	54% (54%)	65% (65%) AIS2+
	cd	5.5 (5.5) mm	13% (13%)	16% (16%) AIS2+
	VC	0.01 (0.01) m/s	1% (1%)	0% (0%) AIS2+
Lumbar Spine	L_{tn}	0 (0) kN	0% (0%)	-
	L_{cm}	4034 (4078) N	63% (64%)	-
Hip	H_{cm}	2.90 (2.76) kN	29% (27.6%)	0% (0%) AIS2+
Femur (thigh)	F_{cm}	0.91 (0.90) kN	9.1% (9%)	0% (0%) AIS2+
Tibia	T_{cm}	84 (83) N	1% (1%)	0% (0%) AIS2+
Tibia	TI	0.69 (0.69)	53% (53%)	5% (5%) AIS2+

In this scenario, the shank (lower leg) of the occupant impacts the structure of the seat pan at around 150 ms, as shown in Figure 14, due to initial braking preceding the FWRB frontal impact. Braking increases the relative velocity of the shank with respect to the seat pan structure leading to increased loading of the tibia.

4. Discussion

The proposed rear-facing seat shows high performance at lower severities (Table 5) as described in Section 3.2.1. The performance of the proposed rear-facing seat at higher severities is discussed in detail in this section. The key restraint system in the proposed rear-facing seat is the torso plate. FWRB frontal impact tests, as shown in Figure 9, pose a challenge for the restraint systems (torso plates, head restraint, energy absorber) since the whole front structure of the car is involved in the crash, creating high decelerations of the occupant compartment.

The risk of head–brain injuries is quite low since the value of HIC_{15} is at most 17% of the IARV, with 0% AIS2+ injury risk and according to BrIC, there is at most 19% AIS1 (minor) injury risk in the worst-case scenario with the occupant leaning forward. The use of a fixed recliner keeps the BrIC values low compared to rotating seatbacks with energy-absorbing recliners [1] since BrIC is associated with head angular velocities.

Considering AIS2+ injuries associated with the upper neck, the injury criteria values are at most 19% of the IARV for the normal sitting posture and at most 24% of the IARV for the out-of-position occupant; this corresponds to about 15% AIS2+ injury risk based on the N_{ij} value. Considering AIS1 (minor) injuries, N_{km} values are at most 67% and 84% of the IARV for the normal sitting posture and the leaning forward posture, respectively. Hence, when the occupant is in the normal sitting posture, the N_{km} value is still below the corresponding capping limit of EuroNCAP (Table 2), which shows the capability of the rear-facing seat to limit whiplash risk even at the highest severity crash pulse NC(64). Considering AIS2+ injuries associated with the lower neck, the injury criteria values are at most 22% of the IARV corresponding to the compression force F_{cmL}. For the normal sitting posture, considering the whole neck based on AIS1 injuries, the injury criteria values are lower than the capping limits specified by EuroNCAP at all severities. For the leaning forward (out-of-position) occupant, considering the whole neck based on AIS1 injuries, upper neck negative shear force (F^{-}_{shU}) and NIC are the only injury criteria whose values are above but close to the capping limits of EuroNCAP at the highest severity crash pulse NC(64). Hence, the out-of-position occupant could survive the highest severity crash with 70% AIS1 (minor) injury based on the NIC value.

Head rebound velocities are about 14% of the IARV, hence are not significant since the recliner is rigid (fixed) and the constant-force deformation element in the energy absorber under the seat is plastically deformed, with minimal elastic rebound.

Noting that the upper torso is restrained by the rigid torso plate, it is imperative to limit distortion (especially S-shape-like distortion) in the neck by using the right amounts of compliance for the head restraint foam, seatback foam and suspension and seat pan foam. Therefore, in order to limit retraction-type distortion in the neck and to be on the safe side, the rear-facing seat with torso plates is designed to induce flexion and protraction in the neck since there is a wider range of motion for protraction in comparison to retraction in the neck in the human body [52]. Hence, $NDI^{(+)}$ values (signifying retraction-type distortion) are kept lower compared to $NDI^{(-)}$ values (signifying protraction-type distortion). The intervertebral angles in the neck are below 30% of the flexion range-of-motion (ROM) and 15% of the extension ROM for the normal sitting posture. For the leaning forward posture, the intervertebral angles in the neck are below 43% of the flexion ROM and 19% of the extension ROM.

At severities lower than that of the crash pulse NC(64), the use of the harder head restraint does not pose any considerable increase in injury risk based on neck distortion and loading as shown by the results in Appendix A. Table A1 indicates that at lower severities, using the harder head restraint slightly increases protraction, leading to a rise in F^{-}_{sh} by an amount from 11 N to 23 N only whereas NIC values increase by 1–7 m^2/s^2, still being close to the higher performance limit. Tables A2–A8 indicate that at higher severities, using the harder head restraint produces very similar responses in comparison to those of the softer head restraint presented in Tables 7–13. At crash pulse NC(47) only, the harder head restraint slightly increases protraction leading to a rise in the negative shear forces ranging

from 24 N to 65 N whereas neck tension forces are reduced by the harder head restraint at higher severities.

For the normal sitting and leaning forward postures, thorax acceleration (Ta_3) is at most 54% of the IARV and this corresponds to at most 65% AIS2+ injury risk. This is an improvement over a comparable study [11] in which a Hybrid III dummy experienced a thorax acceleration of 50 g (84% of the IARV) when it was positioned on a rear-facing seat attached to a sled and subjected to a frontal-impact crash pulse with a delta-V of 60 km/h. The improvement provided by the proposed rear-facing seat is mainly due to the energy absorber under the seat pan. Thorax acceleration is about 50% of the IARV at the highest severity frontal impact since there is limited space in the car for the displacement of the seat pan to absorb the crash energy. At the highest severity, the energy absorber produces a seat pan displacement of 27.8 cm. The net displacement of the seat pan towards the front of the car is reduced to 17.8 cm since the seat is moved 10 cm towards the rear of the car prior to impact. The loading on the thorax and neck can be further reduced by increasing seat pan displacement to absorb more energy if the space in the occupant compartment allows it.

Chest deflection (cd) is at most 7.6% of the IARV, which corresponds to 15% AIS2+ injury risk for the normal sitting posture whereas for the leaning forward posture, chest deflection is at most 13% of the IARV, corresponding to 16% AIS2+ injury risk. Viscous criterion (VC) values are too low to be significant, which means that the rate-dependent injury mechanism is not significant; a similar outcome was obtained in a comparable study [11].

Lumbar tension forces do not develop due to the restriction of the torso by the thorax torso plate. Lumbar compression forces are at most 55% and 64% of the IARV in the normal sitting and leaning forward postures, respectively. In a comparable study [11], a rear-facing seat on a sled (with no torso plates) was subjected to a frontal-impact crash pulse with 60 km/h of delta-V; the resulting lumbar compression forces on the Hybrid III dummy were 81% of the IARV and this was attributed to the upward motion of the torso along the seatback. Considering that the pitching motion of the car is also included in this paper, the proposed rear-facing seat offers an improvement. Lumbar compression forces can be reduced by integrating an energy absorber, which can cushion the impact vertically; this will be the subject of another study.

The results in Tables 13 and 14 indicate that the loading on the hip, femur and tibia does not create any appreciable AIS2+ injury risk. The compression force on the hip is at most 32% of the IARV and the Tibia Index (TI) is at most 53% of the IARV. It should be noted that in the leaning forward posture of the occupant, when the shank is in contact with the seat pan structure and the thigh rotates upward, as seen in Figure 14, there occurs a peak tibia-tension force of 320 N. To the best of the authors' knowledge, there is no established injury probability curve in the literature for tensile loading of the tibia to be used in automotive safety regulations. However, in a recent study [53], the femur (anterior cruciate ligament)–tibial complex failed under tension forces varying between 418 N and 1293 N during tensile loading of fresh specimens obtained from cadavers aged between 60 and 70 years. Although the IARVs in Table 6 are based on volunteer and cadaver tests, it is advised that an updated set of IARVs should also include tibia tension forces for rear-facing occupants subjected to frontal impacts.

Crash scenarios where the seat loads the occupant are investigated in this paper. It is believed that in order to make continuous progress in occupant safety, protection (restraint) systems should be designed and tested using any human-body model suitable for this type of loading. The human-body model [15,16] used in this paper was built using volunteer and cadaver data in order to design seats to mitigate whiplash risk in rear impacts. The restraint systems, including the energy-absorber under the seat pan are designed such that the seat cushions the impact and the relative movements between human-body parts are restricted. Due to the use of torso plates, the joint rotations in the thoracic and lumbar spines are at most 38% and 50% of the corresponding ROMs considering both flexion and extension of the spine. The results in this paper indicate that, in the worst-case scenario,

the values of the injury criteria based on the loading on the neck do not substantially exceed the capping limits of the EuroNCAP whiplash protocol. Moreover, in the normal sitting posture, the injury criteria values are lower than the capping limits at all severities. Therefore, the human-body model employed in this study can be confidently used to investigate high-severity crash scenarios as long as the severity of the crash is mitigated by designing a protection system, as performed in this study.

The responses of the rear-facing seat-occupant model presented in this study are verified using the experimental data given in a comparable study by Zellmer and Manneck [11], where a rear-facing generic seat attached to a sled was subjected to a frontal impact crash pulse using a 50th percentile male Hybrid III dummy. The experimental study by Zellmer and Manneck [11] is the only comparable study to verify the responses of the rear-facing seat-occupant model. The experimental study and the rear-facing seat-occupant simulation in this study are quite similar based on delta-V (around 60 km/h), initial seatback angle, initial sitting posture, type of seat foam and the use of an integrated seatbelt. Both the occupant model and the Hybrid III dummy had zero backsets between the head and the head restraint before impact. The human-body model (occupant model) in this study has a realistic kyphotic thoracic spine which is multi-segmented; on the other hand, the Hybrid III dummy has a more flat and rigid thoracic spine that does not allow spine extension. For this reason, in the experimental study, the thorax of the Hybrid III dummy was in full contact with the seatback without any significant gap between the upper torso and the upper seatback at the start of the impact and during the loading phase of the impact. Similarly, in the rear-facing seat proposed in this study are torso plates that restrict the motion of the torso relative to the seatback, and also suppress spine extension. In the experimental study, energy absorption was provided by the rotation of the seatback by a maximum amount of 16 deg. Table A9 in Appendix A presents a comparison between the simulation and the experimental data in terms of injury risk expressed in % IARV. The criteria common to both studies are presented in Table A9. Mean $\pm$ one standard deviation values are given for the experimental data. The experimental data show some variation due to repeatability issues, as the experimental sled test was performed several times. It can be seen that there is good agreement between simulation and experimental results, except for a few responses. The differences in some responses are due to the considerable rebound of the seatback in the experimental study and the structural differences in the neck of the human-body model and the Hybrid III dummy. The considerable rebound of the seatback in the experimental study stems from the fact that the rotation of the seatback is controlled solely by the elasticity of two layers of seatbelt webbing mounted between the upper seatback and the frame mounted on the sled. The rear-facing seat-occupant model produces lower injury risks (lower % IARV) overall due to the improved protection offered by the proposed rear-facing seat. Considering that different human models and dummies can exhibit some significant variations in responses under the same test conditions [12], the simulation and experimental results are quite comparable in terms of order of magnitude.

Although pre-crash braking enables the head and upper torso to align with the head restraint and torso plates, the rear-facing seat offers the best protection when the occupant is in the normal sitting posture, as shown in Figure 8. Therefore, if the occupant is out-of-position and there is a risk of a crash, the posture of the occupant should be corrected in a timely manner prior to impact by activating an auditory signal to warn the occupant or by using motorised seatbelts that provide pre-pretensioning of the seatbelt [1,54]. With autonomous vehicle technology and Advanced Driver-Assistance Systems (ADAS), there will always be automatic braking and measures to evade accidents together with the correction of occupant posture before impact. Hence, it is expected that the chances of having the highest severity crash as shown in Figure 14 will be very much reduced.

It Is shown that when the proposed rear-facing seat with torso plates is reversed to be used as a forward-facing seat, it offers good whiplash protection in rear impacts when the occupant has the normal sitting posture before impact. If the proposed seat with torso plates is to be used as a forward-facing seat as well, rear impact simulations with pre-crash Automated Emergency Braking (AEB) and pre-pretensioning of the seatbelt need to be performed to check the performance of the seat [55].

5. Conclusions

Travelling in rear-facing seats can be an option in future autonomous cars. However, frontal impacts that can occur with higher severities compared with rear impacts can cause a higher risk of whiplash. The first part of this study demonstrated that a forward-facing anti-whiplash seat that employs state-of-the-art occupant protection technology can mitigate whiplash risk in rear impacts and earn maximum points from the EuroNCAP whiplash protocol. However, when this forward-facing seat is reversed for use as a rear-facing seat, it cannot offer adequate protection against whiplash. Therefore, this paper presents an improved rear-facing seat design involving two torso plates, a fixed recliner and an energy absorber under the seat pan. The simulation results indicate that the proposed rear-facing seat offers good protection for the whole human-body (50th percentile male) since the injury criteria values are considerably lower than the injury assessment reference values for AIS2+ injuries at all severities. Moreover, for the normal sitting posture, the neck injury criteria values are lower than the capping limits specified by EuroNCAP at all severities studied in this paper. The torso plates work in unison with the head restraint and energy absorber under the seat pan to reduce loads on the neck and limit neck distortion. The Neck Distortion Index (NDI), which is a seat design tool, is employed to monitor neck distortions during the design optimisation of the seats. It is important that occupants should be willing to use these torso plates.

This study presents a comprehensive portrayal of crash scenarios in which the seat loads the occupant. It is shown that it is difficult to protect a rear-facing occupant subjected to frontal impact with delta-Vs reaching 64 km/h and at the same time satisfy the whiplash assessment criteria of EuroNCAP specified for rear-end collisions with delta-Vs lower than 25 km/h. Therefore, this study proposes the restriction of head, neck and torso motion by using torso plates, head restraints and fixed recliners so that the occupant moves almost as a whole with the seat. It is considered that this study can be a useful reference for seat designers since detailed mechanical properties of seats, as given in this paper, are scarce in the literature.

Author Contributions: Conceptualization, S.H.; methodology, S.H.; software, S.H. and S.Y.; validation, S.H. and S.Y.; formal analysis, S.H. and S.Y.; investigation, S.H. and S.Y.; resources, S.H. and S.Y.; data curation, S.H. and S.Y.; writing—original draft preparation, S.H. and S.Y.; writing—review and editing, S.H. and S.Y.; visualization, S.H. and S.Y.; supervision, S.H. and S.Y.; project administration, S.H.; funding acquisition, S.H. and S.Y. All authors have read and agreed to the published version of the manuscript.

Funding: This research received no external funding.

Data Availability Statement: Data is contained within the article.

Acknowledgments: The authors thank Oguzhan Gultekin and Bilal Toprak for their assistance with running the FE simulations.

Conflicts of Interest: The authors declare no conflict of interest.

Appendix A

Table A1. Performance of the proposed seat (with torso plates and the harder head restraint) at lower severities. The occupant is in the normal sitting posture.

Pulse	NIC	N_{km}	v_r	F_{sh}^{+}	F_{sh}^{-}	F_{tn}	M_{yU}	F_{shL}	M_{yL}	T1a	HrCt	NDI$^{(-)}$	NDI$^{(+)}$
SN(9.4)	8.83	0.19	0.48	17.7	102	69	3.01	96	3.42	6.79	15	2.52	0.28
SN(13)	16.8	0.28	0.42	20.0	146	44	4.97	139	5.00	9.07	9	2.18	0.17
SN(16)	17.2	0.31	0.43	15.0	153	75	4.51	135	4.63	8.83	17	2.72	0.29
SN(20)	16.4	0.28	0.39	13.9	134	20	5.01	108	4.05	7.95	12	3.05	0.21
TR(24)	14.5	0.28	0.39	11.9	142	77	4.68	119	4.76	8.59	11	2.42	0.21

Table A2. Rear-facing seat performance with the harder head restraint at higher severities (head). The occupant is in the normal sitting posture.

Pulse	HIC_{15}	BrIC
HS(35)	7.91 (1.1% IARV) (0% AIS2+)	0.05 (7% AIS1, 0% AIS2)
NC(47)	35.8 (5.1% IARV) (0% AIS2+)	0.06 (11% AIS1, 0.1% AIS2)

Table A3. Rear-facing seat performance with harder head restraint at higher severities (upper neck). The occupant is in the normal sitting posture.

Pulse	N_{km}	F_{shU}^{+}	F_{shU}^{-}	F_{tnU}	F_{cmU}	M_{yUE}	M_{yUF}	N_{ij}
HS(35)	0.31 (31% IARV)	19 (0.6% IARV)	172 (5.5% IARV)	94.3 (2.8% IARV)	385 (9.6% IARV)	5.46 (9.5% IARV)	0.83 (0.4% IARV)	0.12 (13% AIS2+) (12% IARV)
NC(47)	0.49 (49% IARV)	15 (0.5% IARV)	287 (9.2% IARV)	93 (2.8% IARV)	653 (16% IARV)	7.82 (14% IARV)	1.01 (0.5% IARV)	0.16 (13% AIS2+) (16% IARV)

Table A4. Rear-facing seat performance with harder head restraint at higher severities (lower neck). The occupant is in the normal sitting posture.

Pulse	F_{shL}^{+}	F_{shL}^{-}	F_{tnL}	F_{cmL}	M_{yLE}	M_{yLF}
HS(35)	41.7 (1.3% IARV)	142 (4.6% IARV)	84.9 (2.6% IARV)	412 (10% IARV)	3.29 (1.7% IARV)	5.47 (1.4% IARV)
NC(47)	103 (3.3% IARV)	157 (5% IARV)	77 (2.3% IARV)	739 (18% IARV)	3.52 (1.8% IARV)	6.41 (1.7% IARV)

Table A5. Rear-facing seat performance with the harder head restraint at higher severities (overall neck). The occupant is in the normal sitting posture.

Pulse	v_r	NIC	NDI$^{(-)}$	NDI$^{(+)}$
HS(35)	0.39 (6.5% IARV)	21 (78% IARV)	3.34	0.14
NC(47)	0.54 (9% IARV)	9.9 (37% IARV)	5.50	0.25

Table A6. Rear-facing seat performance with harder head restraint at higher severities (thorax). The occupant is in the normal sitting posture.

Pulse	Ta_3	cd	VC
HS(35)	12.3 (20.5% IARV) (37% AIS2+)	2.3 (5.5% IARV) (14% AIS2+)	0.0059 (0.59% IARV) (0% AIS2+)
NC(47)	24.8 (41% IARV) (55% AIS2+)	2.5 (6% IARV) (14% AIS2+)	0.0054 (0.54% IARV) (0% AIS2+)

Table A7. Rear-facing seat performance with harder head restraint at higher severities (lumbar spine). The occupant is in the normal sitting posture.

Pulse	L_{tn}	L_{cm}
HS(35)	0	2002 (31% IARV)
NC(47)	0	2817 (44% IARV)

Table A8. Rear-facing seat performance with harder head restraint at higher severities (hip–femur–tibia). The occupant is in the normal sitting posture.

Pulse	H_{cm}	F_{cm}	T_{cm}	TI
HS(35)	1.3 (13% IARV) (0% AIS2+)	0.21 (2.1% IARV) (0% AIS2+)	43 N (0.54% IARV) (0% AIS2+)	0.063 (4.8% IARV) (0% AIS2+)
NC(47)	2.18 (21.8% IARV) (0% AIS2+)	0.42 (4.2% IARV) (0% AIS2+)	45 N (0.56% IARV) (0% AIS2+)	0.11 (8.5% IARV) (0% AIS2+)

Table A9. Comparison of the rear-facing seat-occupant model simulation with experimental data (exp) from the Hybrid III dummy [11].

Region	Criterion	% IARV-exp	% IARV-Model
Head	HIC_{15}	70–80%	13%
Upper Neck	F^{+}_{shU}	1–1.5%	0.4%
	F^{-}_{shU}	23–32%	11%
	F_{tnU}	8–13%	13%
	F_{cmU}	25–35%	18%
	M_{yUE}	19–43%	19%
	M_{yUF}	17–18%	3%
	N_{ij}	18–38%	19%
Lower Neck	F^{+}_{shL}	36–40%	10%
	F^{-}_{shL}	10–15%	4.8%
	F_{tnL}	17–19%	5.4%
	F_{cmL}	20–23%	21%
	M_{yLE}	1–1.5%	7.2%
	M_{yLF}	17–18%	1.6%
Thorax	Ta_3	85–90%	54%
	cd	18–20%	15%
	VC	2–3%	0.6%
Lumbar Spine	L_{tn}	7–10%	0%
	L_{cm}	74–91%	55%

References

1. Himmetoğlu, S. Introduction of a Protection System for Rear-Facing Seats in Autonomous Car Crashes. In Proceedings of the 26th International Scientific Conference Transport Means, Kaunas, Lithuania, 5–7 October 2022; pp. 104–109.
2. Gutsche, A.J.; Tomasch, E.; Sinz, W.; Levallois, I.; Alonso, S.; Lemmen, P.; Linder, A.; Steffan, H. Improve Assessment and Enhance Safety for the Evaluation of Whiplash Protection Systems Addressing Male and Female Occupants in Different Seat Configurations by Introducing Virtual Methods in Consumer Tests. In Proceedings of the 2013 Ircobi Conference, Göteborg, Sweden, 11–13 September 2013; pp. 77–90.
3. Jakobsson, L.; Östh, J.; Bohman, K. Rear-end Impact Assessment Expanded with Pre-Impact Posture Variations. In Proceedings of the 2021 Ircobi Conference, Online, 8–10 September 2021.
4. Parenteau, C.S.; Viano, D.C.; Lau, E.C. Rear-Seat occupant demographics in rear impacts. *Traffic Inj. Prev.* **2021**, *22*, 218–223. [CrossRef] [PubMed]
5. EuroNCAP. *European New Car Assessment Programme–The Dynamic Assessment of Car Seats for Neck Injury Protection Testing Protocol*; Version 4.1.1; EuroNCAP: Leuven, Belgium, 2021; 54p.
6. National Highway Traffic Safety Administration (NHTSA). Available online: www.nhtsa.gov/research-data/research-testing-databases#/vehicle (accessed on 11 September 2023).
7. Jakobsson, L.; Isaksson-Hellman, I.; Lindman, M. WHIPS (Volvo Cars' Whiplash Protection System)—The development and real-world performance. *Traffic Inj. Prev.* **2008**, *9*, 600–605. [CrossRef] [PubMed]
8. Mang, D.W.H.; Siegmund, G.P.; Blouin, J.-S. A comparison of anti-whiplash seats during low/moderate speed rear-end collisions. *Traffic Inj. Prev.* **2020**, *21*, 195–200. [CrossRef] [PubMed]
9. Himmetoglu, S.; Acar, M.; Bouazza-Marouf, K.; Taylor, A.J. Car-seat design to improve rear-impact protection. *Proc. IMechE Part D J. Automob. Eng.* **2011**, *225*, 441–459. [CrossRef]
10. Zellmer, H.; Lubbe, N.; Sander, U. Assessing the Injury Risk of Car Occupants on Rearward Facing Seats–An Analysis of GIDAS Cases. In Proceedings of the 8th ESAR Expert Symposium on Accident Research Conference, Hannover, Germany, 19–20 April 2018.
11. Zellmer, H.; Manneck, F. Assessing Injury Risk of Car Occupants on Rearward Facing Seats in a Full Frontal Impact–Sled Tests in a Generic Test Environment. In Proceedings of the 26th ESV Conference, Eindhoven, The Netherlands, 10–13 June 2019.
12. Soni, A.; Schilling, S.; Faust, J.; Eickhoff, B. Responses of HIII, THOR, and SAFER-HBM Occupant Models in Rearward-Facing Seat Configuration for High Severity Frontal Impact. In Proceedings of the 2020 Ircobi Conference, Munich, Germany; 2020.
13. Jin, X.; Hou, H.; Shen, M.; Wu, H.; Yang, K.H. Occupant Kinematics and Biomechanics with Rotatable Seat in Autonomous Vehicle Collision: A Preliminary Concept and Strategy. In Proceedings of the 2018 Ircobi Conference, Athens, Greece, 12–14 September 2018.
14. Hasija, V.; Kelkar, R.; Takhounts, E.G. Simulation Assessment of Injury Trends for 50th Percentile Males Using Potential Seating Configurations of Future Automated Driving System (ADS) Equipped Vehicles. In Proceedings of the 26th ESV Conference, Eindhoven, The Netherlands, 10–13 June 2019.
15. Himmetoglu, S.; Acar, M.; Bouazza-Marouf, K.; Taylor, A.J. A multibody human model for rear-impact simulation. *Proc. IMechE Part D J. Automob. Eng.* **2009**, *223*, 623–638. [CrossRef]
16. Himmetoglu, S. Validation of a Multi-Body Human Model for Efficient Rear Impact Simulations. In Proceedings of the 25th International Scientific Conference Transport Means 2021, Online/Kaunas, Lithuania, 6–8 October 2021; pp. 35–40.
17. Davidsson, J.; Ono, K.; Inami, S.; Svensson, M.Y.; Lövsund, P. A Comparison between Volunteer, BioRID P3 and Hybrid III Performance in Rear Impacts. In Proceedings of the 1999 Ircobi Conference, Sitges, Spain, 23–24 September 1999; pp. 165–178.
18. Insurance Institute for Highway Safety. *Insurance Institute for Highway Safety–Vehicle Seat/Head Restraint Evaluation Protocol–Dynamic Criteria*; Version V; IIHS: Ruckersville, VA, USA, 2019; 31p.
19. Kolich, M. Occupant preferred back angle relative to head restraint regulations. *SAE Int. J. Passeng. Cars* **2010**, *3*, 626–632. [CrossRef]
20. Karabeyoglu, C. Smart Car Seat Design for Safety and Comfort. Master's Thesis, Hacettepe University, Mechanical Engineering Department, Ankara, Turkey, 2019.
21. Edwards, M.A.; Brumbelow, M.L.; Trempel, R.E.; Gorjanc, T.C. Seat Design Characteristics Affecting Occupant Safety in Low- and High-Severity Rear-Impact Collisions. In Proceedings of the 2019 Ircobi Conference, Florence, Italy, 11–13 September 2019.
22. Wietholter, K.; Echemendia, C.; Louden, A.E. Development of a Representative Seat Assembly for FMVSS No. 213. In Proceedings of the 25th ESV Conference, Detroit, MI, USA, 5–8 June 2017.
23. Genzel, J.; Carlsson, A.; Linder, A.; Pipkorn, B.; Svensson, M. An Open-Source Finite Element Model of a Generic Car Seat: Development and Validation for Low-Severity Rear Impact Evaluations. In Proceedings of the 2022 Ircobi Conference, Porto, Portugal, 14–16 September 2022.
24. Viano, D.C. *Role of the Seat in Rear Crash Safety*; Society of Automotive Engineers: Warrendale, PA, USA, 2002.
25. Netherlands' Organization for Applied Research (TNO). *MADYMO Theory Manual*; Version 6.2.2; TNO MADYMO BV: Delft, The Netherlands, 2005.
26. Park, C.K.; Kan, C.D. Objective Evaluation Method of Vehicle Crash Pulse Severity in Frontal New Car Assessment Program (NCAP) Tests. In Proceedings of the 24th ESV Conference, Gothenburg, Sweden, 8–11 June 2015.

27. Gabauer, D.J.; Gabler, H.C. Can Delta-V be Adjusted with Structural and Occupant Restraint Performance to Improve Prediction of Chest Acceleration? In Proceedings of the Annals of Advances in Automotive Medicine, 52nd Annual Scientific Conference, San Diego, CA, USA, 6–8 October 2008.
28. Zuby, D.S.; Farmer, C.M.; Avery, M. The Influence of Crash Pulse Shape on BioRID Response. In Proceedings of the 2003 Ircobi Conference, Lisbon, Portugal, 25–26 September 2003; pp. 327–341.
29. Wood, D.P.; Adamson, D.; Ydenius, A. Car frontal collisions: Occupant compartment forces, interface forces and stiffnesses. *Int. J. Crashworthiness* **2004**, *9*, 311–325. [CrossRef]
30. EuroNCAP. *European New Car Assessment Programme–Assessment Protocol–Adult Occupant Protection*; Version 9.1.3; EuroNCAP: Leuven, Belgium, 2021; 49p.
31. Himmetoglu, S. An Evaluation of Passive Head-Restraints with Different Stiffness and Energy Dissipation Properties for Whiplash Mitigation. In Proceedings of the 7th International Expert Symposium on Accident Research (ESAR 2016), Hannover, Germany, 9–10 June 2016.
32. Hu, D.Y.; Yang, J.L.; Hu, M.H. Full-scale vertical drop test and numerical simulation of a crashworthy helicopter seat/occupant system. *Int. J. Crashworthiness* **2009**, *14*, 565–583. [CrossRef]
33. Desjardins, S.P. The Evolution of Energy Absorption Systems for Crashworthy Helicopter Seats. In Proceedings of the American Helicopter Society 59th Annual Forum, Phoenix, AZ, USA, 6–8 May 2003.
34. Zhang, X.; Zhou, Q. An energy-absorbing sliding seat for reducing neck injury risks in rear impact–analysis for prototype built. *Traffic Inj. Prev.* **2016**, *17*, 313–319. [CrossRef] [PubMed]
35. Östling, M.; Lundgren, C.; Lubbe, N.; Pipkorn, B. Reducing lumbar spine vertebra fracture risk with an adaptive seat track load limiter. *Front. Future Transp.* **2022**, *3*, 1–10. [CrossRef]
36. Jazar, R.N. *Vehicle Dynamics: Theory and Application*; Springer Science + Business Media LLC.: New York, NY, USA, 2008.
37. Marzougui, D.; Samaha, R.R.; Cui, C.; Kan, C.-D. *Working Paper NCAC 2012-W-005*; National Crash Analysis Center (NCAC); The George Washington University: Washington, DC, USA, 2012.
38. Society of Automotive Engineers (SAE). *SAE J211-1 (1995): Instrumentation for Impact Test, Part 1, Electronic Instrumentation*; SAE: Warrendale, PA, USA, 2007.
39. Schmitt, K.U.; Niederer, P.F.; Cronin, D.S.; Morrison, B., III; Muser, M.H.; Walz, F. *Trauma Biomechanics*, 5th ed.; Springer Nature: Cham, Switzerland, 2019.
40. Takhounts, E.G.; Craig, M.J.; Moorhouse, K.; McFadden, J.; Hasija, V. Development of brain injury criteria (BrIC). *Stapp Car Crash J.* **2013**, *57*, 243–266. [CrossRef] [PubMed]
41. Eppinger, R.; Sun, E.; Bandak, F.; Haffner, M.; Khaewpong, N.; Maltese, M.; Kuppa, S.; Nguyen, T.; Takhounts, E.; Tannous, R.; et al. *Development of Improved Injury Criteria for the Assessment of Advanced Automotive Restraint Systems—II*; NHTSA: Washington DC, USA, 1999.
42. Rupp, J.D.; Flannagan, C.A.C.; Kuppa, A.M. *Development of New Injury Risk Curves for the Knee/Distal Femur and the Hip for Use in Frontal Impact Testing*; Report No. UMTRI-2009-08; The University of Michigan Transportation Research Institute: Ann Arbor, MI, USA, 2009.
43. Kuppa, S.; Wang, J.; Haffner, M.; Eppinger, R. Lower Extremity Injuries and Associated Injury Criteria. In Proceedings of the 17th ESV Conference, Amsterdam, The Netherlands, 4–7 June 2001.
44. Lau, I.V.; Viano, D.C. The Viscous Criterion—Bases and applications of an injury severity index for soft tissues. *SAE Trans.* **1986**, *95*, 672–691. [CrossRef]
45. Bracq, A.; Delille, R.; Marechal, C.; Bourel, B.; Roth, S.; Mauzac, O. Rib fractures prediction method for kinetic energy projectile impact: From blunt ballistic experiments on SEBS gel to impact modeling on a human torso FE model. *Forensic Sci. Int.* **2019**, *297*, 177–183. [CrossRef] [PubMed]
46. Funk, J.R.; Rudd, R.W.; Kerrigan, J.R.; Crandall, J.R. Analysis of Tibial Curvature, Fibular Loading, and the Tibia Index. In Proceedings of the 2003 Ircobi Conference, Lisbon, Portugal, 25–26 September 2003; pp. 135–147.
47. Yoganandan, N.; Arun, M.W.J.; Stemper, B.D.; Pintar, F.A.; Maiman, D.J. Biomechanics of human thoracolumbar spinal column trauma from vertical impact loading. *Ann. Adv. Automot. Med.* **2013**, *57*, 155–166. [PubMed]
48. Boström, O.; Bohman, K.; Haland, Y.; Kullgren, A.; Krafft, M. New AIS1 Long-Term Neck Injury Criteria Candidates Based on Real Frontal Crash Analysis. In Proceedings of the 2000 IRCOBI Conference, Montpellier, France, 20–22 September 2000; pp. 249–264.
49. Ejima, S.; Zama, Y.; Satou, F.; Holcombe, S.; Ono, K.; Kaneoka, K.; Shiina, I. Prediction of the Physical Motion of the Human Body Based on Muscle Activity During Pre-Impact Braking. In Proceedings of the 2008 Ircobi Conference, Bern, Switzerland, 17–19 September 2008; pp. 163–175.
50. Erlinger, N.; Kofler, D.; Heider, E.; Klug, C. Effects of Boundary Conditions and Posture on Simulations with Human Body Models of Braking Events. In Proceedings of the 2022 Ircobi Conference, Porto, Portugal, 14–16 September 2022.
51. Karemyr, M.; Pettersson, T.; Svensson, M.; Linder, A. *Development of Prototype Concepts of the SETs of an Average Female and Male for Low Severity Rear Impact Crash Testing*; VTI Report 1147A; Swedish National Road and Transport Research Institute (VTI): Linköping, Sweden, 2022.
52. Severinsson, Y.; Elisson, L.; Bunketorp, O. Reliability of measuring the cervical sagittal translation mobility with a simple method in a clinical setting. *Rehab. Res. Prac.* **2012**, *2012*, 629104. [CrossRef] [PubMed]

53. Marieswaran, M.; Mansoori, N.; Digge, V.K.; Jhajhria, S.K.; Behera, C.; Lalwani, S.; Kalyanasundaram, D. Effect of preservation methods on tensile properties of human femur-acl-tibial complex (FATC)—A Cadaveric Study on Male Subjects. *Acta Bioeng. Biomech.* **2018**, *20*, 31–42. [PubMed]
54. Graci, V.; Griffith, M.; Seacrist, T.; Brase, D.; Mishra, E.; Pipkorn, B.; Lubbe, N.; Arbogast, K.B. Repositioning forward-leaning vehicle occupants with a pre-pretensioner belt and a startle-based warning in pre-crash scenarios. *Traffic Inj. Prev.* **2022**, *23*, 32–37. [CrossRef] [PubMed]
55. Mishra, E.; Mroz, K.; Lubbe, N. Repositioning forward-leaning passengers by seatbelt pre-pretensioning. *Traffic Inj. Prev.* **2023**, *24*, 716–721. [CrossRef] [PubMed]